Characterization of materials with elastic scattering experiments using MeV protons and α-particles beams

Valentino Rigato
Laboratori Nazionali Legnaro LNL– INFN
valentino.rigato@lnl.infn.it

The lesson will briefly outline the features and examples of use of the non-destructive micro-analytical techniques based on elastic scattering with proton and alpha particle MeV ions, i.e. Rutherford and non-Rutherford Backscattering Spectrometry (shortly EBS), which are widely used for the characterization of surfaces, interfaces, thin films, elemental depth profiling and impurity concentration analysis in many research and industrial fields.

OUTLINE

- Introduction
- Cross section
- Kinematics of elastic collisions
- Energy loss and Energy Straggling
- Mass separation, depth resolution
- Application examples in material research

ION BEAM ANALYSIS (IBA)

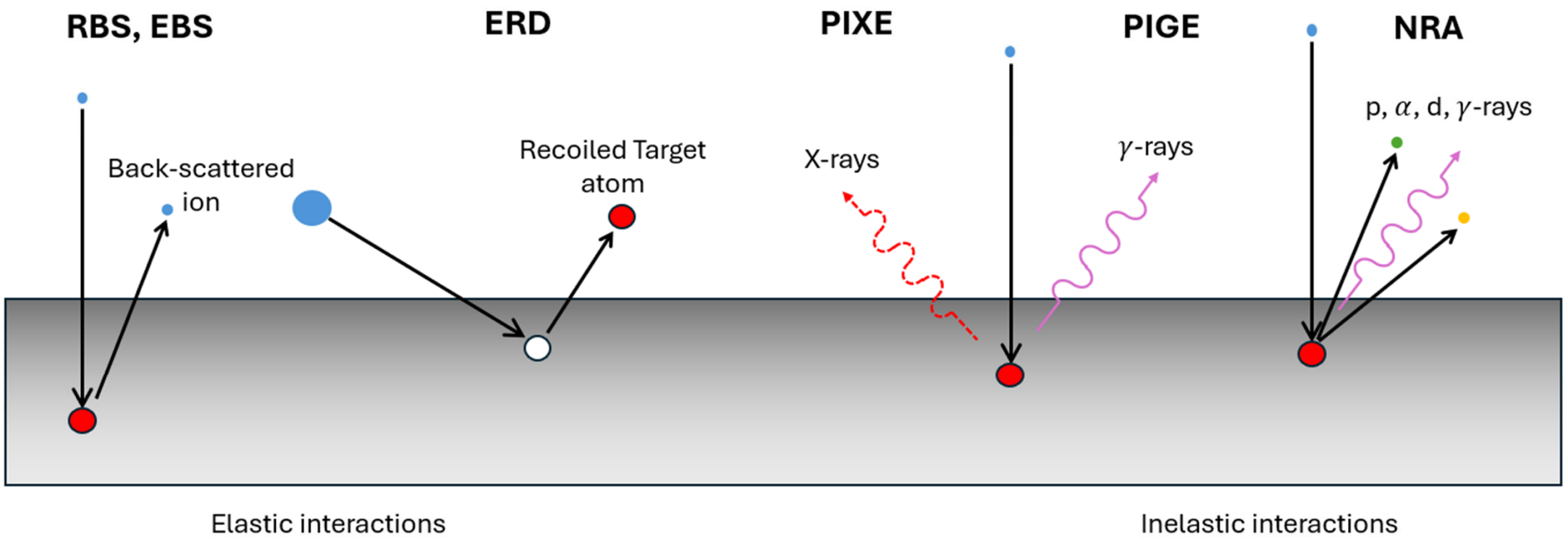

Elastic scattering techniques: RBS, EBS, ERD

Today firmly established as quantitative and versatile techniques of Ion Beam Analysis.

Used in semiconductor, space, metellurgical, energy and quantum and nano-technology and other industrial fields

Advantages:

I. Quantitative analysis (typically 2-5%) for almost all elements without requiring calibrated standards. They are used to calibrate standards for other micro-analytical techniques.

II. Provide mass resolution (hence elemental discrimination) of near-surface impurities

III. Very sensitive to heavy elements (ppm)

IV. Less sensitive to light elements (other NRA IBA are used in parallel)

V. Analysed depth (typical for MeV proton and α particles): 2 μm (α), 20 μm (protons)

VI. Excellent depth resolution (eg: 2-5 nm under optimal conditions)

VII. Non destructive

VIII. Ideal techniques for atom-site location in single crystal targets (in combination with channeling) and for elemental depth profile determination in layered structures, diffusion studies, ion mixing, interface analysis, thickness determination ...)

Elastic scattering techniques: RBS, EBS, ERD

- Use MeV electrostatic / Van de Graaff accelerators
- High vacuum scattering chambers and beam-lines
- Specific particles detectors
- Fast, reliable, stable electronics for signal processing
- Modern DAQ hardware and software

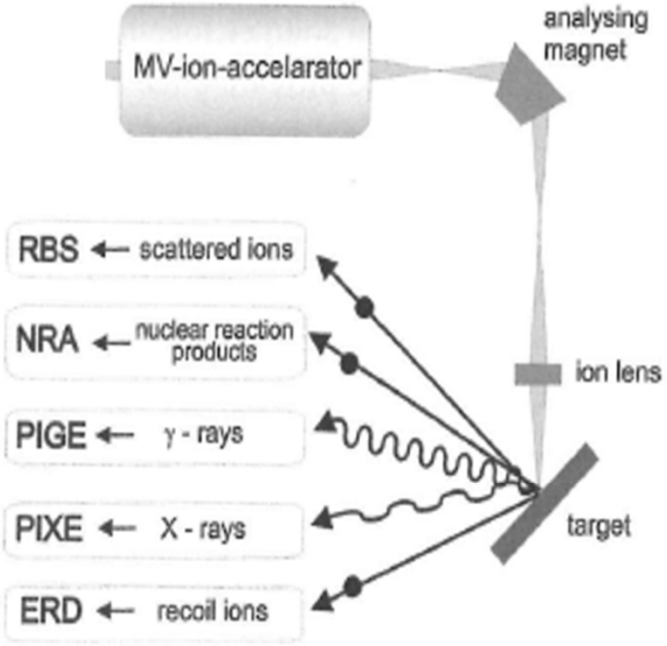

Simplified illustration of the equipment used for EBS

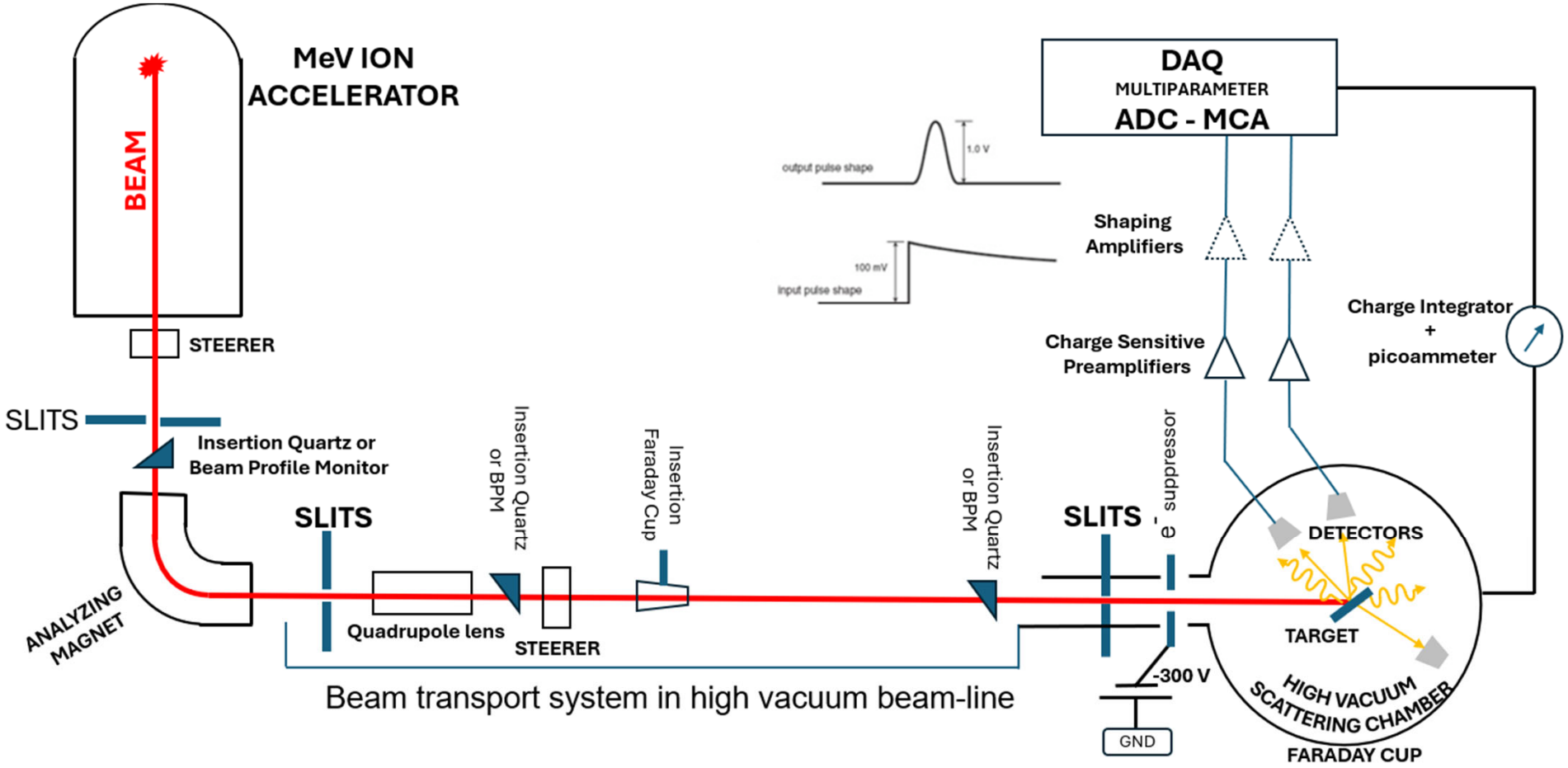

Rutherford cross section.
Interaction between two point-like charges

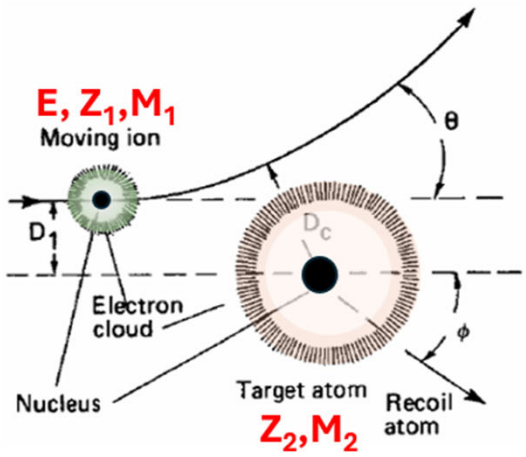

Assumptions

- Point-like charged particles
- Neglect shielding of electron cloud
- Distance of closest approach large enough that nuclear force is negligible

For the COULOMB INTERACTION, a central force field, the differential scattering cross section of a target atom for scattering an incident particle through an angle θ into a differential solid angle dΩ centered about θ, in the laboratory frame of reference is given by:

$$\frac{d\sigma}{d\Omega} = \left(\frac{Z_1 Z_2 e^2}{2E\sin^2\theta}\right)^2 \frac{[\cos\theta + (1 - \mu^2\sin^2\theta)^{1/2}]^2}{(1 - \mu^2\sin^2\theta)^{1/2}}$$

$\mu = M_1/M_2$

E = energy of the projectile immediately before scattering

For particles with energy around 0.4-0.5 MeV/amu Rutherford cross section gives very accurate (2%) measurements for medium-high atomic number elements.

Rutherford cross section

$$\frac{d\sigma}{d\Omega} = \left(\frac{Z_1 Z_2 e^2}{2E\sin^2\theta}\right)^2 \frac{[\cos\theta + (1 - \mu^2\sin^2\theta)^{1/2}]^2}{(1 - \mu^2\sin^2\theta)^{1/2}}$$

$\mu = M_1/M_2$

E = energy of the projectile immediately before scattering

Note: sensitivity is enanced by **factor $(Z_2/E)^2$**

- High Z elements have much higher cross section
- Incresing energy will reduce sensitivity

The Rutehrford cross section provides a very accurate yield estimate (2%) for almost all target atoms provided that the beam energy does not exceed **about 0.4-0.5 MeV per atomic mass unit.**

Complex and large deviations (resonances) from the Rutherford value are observed for H and He ions, as a consequence of nuclear interaction, particularly in low atomic number target elements, in the entire energy range from few tens keV to 10 MeV.

1-2 MeV $^4He^+$ beams are commonly used for RBS to avoid such deviations.

With protons at energies 1-2 MeV some deviation are observed (depending of specific conditions) and may be used for EBS analyses.

With higher Z ions, the true scattering cross section is always slighgly lower that the Rutherford value due to the screening effect of the atomic electrons.
The screening corrections can be calculated quite accurately and must enter in the Yield calculation

Solid angle of the detector

In backscattering spectrometry, the detector solid angle Ω is small (about 10^{-3} steradians) so that one defines an average differential scattering cross section:

$$\sigma(E,\theta) = (1/\Omega)\int_{\Omega}(d\sigma/d\Omega)d\Omega$$

KINEMATICS OF ELASTIC COLLISIONS

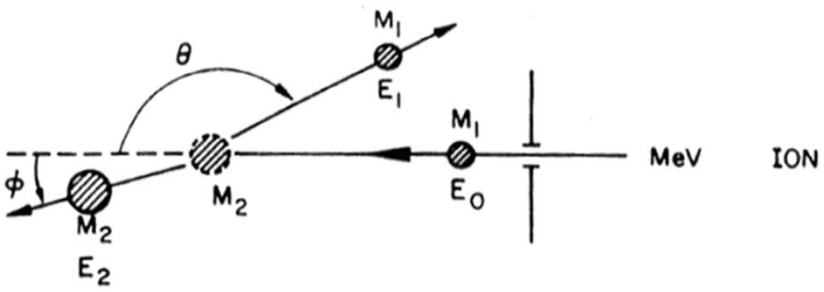

Schematic representation of an elastic collision between a projectile of mass M_1 and energy E_0 and a target mass M_2 which is initially at rest. After the collision, the projectile and target mass have energies E_1 and E_2 respectively. The angles θ and ϕ are positive as shown.
All quantities refer to a laboratory frame of reference.

Reactions are written in the format

X(a,b)Y

which is to be translated

TARGET NUCLEUS (*projectile*, *emitted particle*) RESIDUAL NUCLEUS

In an elastic reaction a=b, X=Y

Examples:

$Ta(^4He,^4He)Ta$ same as $Ta(\alpha,\alpha)Ta$

$^{12}C(p,p)^{12}C$ same as $^{12}C(^1H,\ ^1H)^{12}C$

Kinematic coefficient

For $M_1 < M_2$, conservation of energy and momentum, gives:

$$\frac{E_1}{E_0} = \left[\frac{(M_2^2 - M_1^2\sin^2\theta)^{1/2} + M_1\cos\theta}{M_1 + M_2}\right]^2$$

$$E_1 = K_{M_2} E_0$$

K_{M_2} = kinematic factor

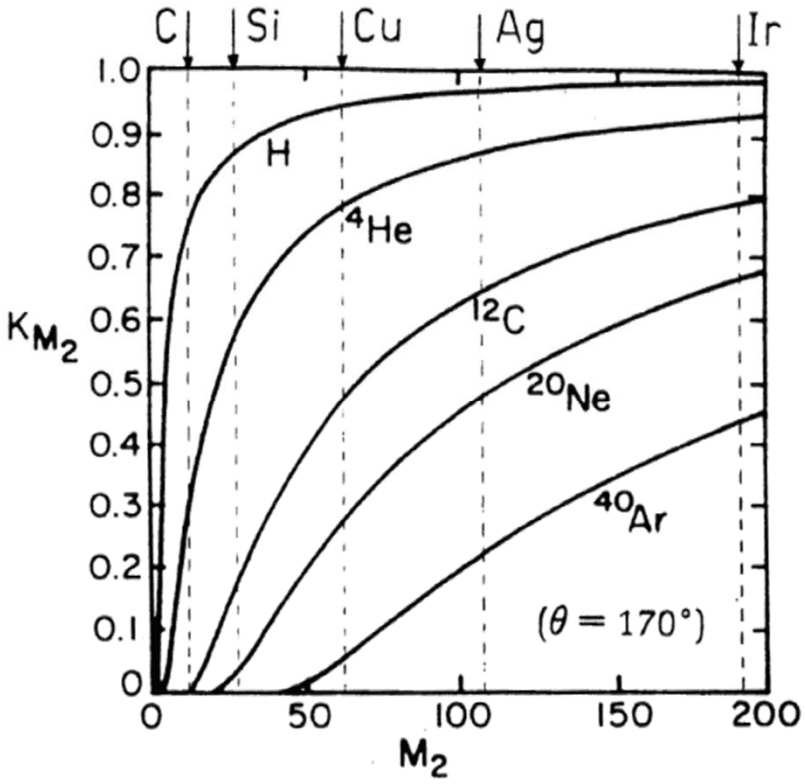

One reason to work in back-scattering geometry

Two different atoms , A and B, with masses M_A and M_B, are distinguished if the energy difference:

$$\Delta E_1 = E_1(M_A) - E_1(M_B) = (K_{M_A} - K_{M_B})E_0$$

is larger than the energy resolution of the whole detecting apparatus (detector + electronics).

$(K_{M_A} - K_{M_B})$ increases as the scattering angle increases:

Best mass resolution is obtained by choosing a scattering angle in back-word direction (BACK-SCATTERING), preferably in the range 150°-180°

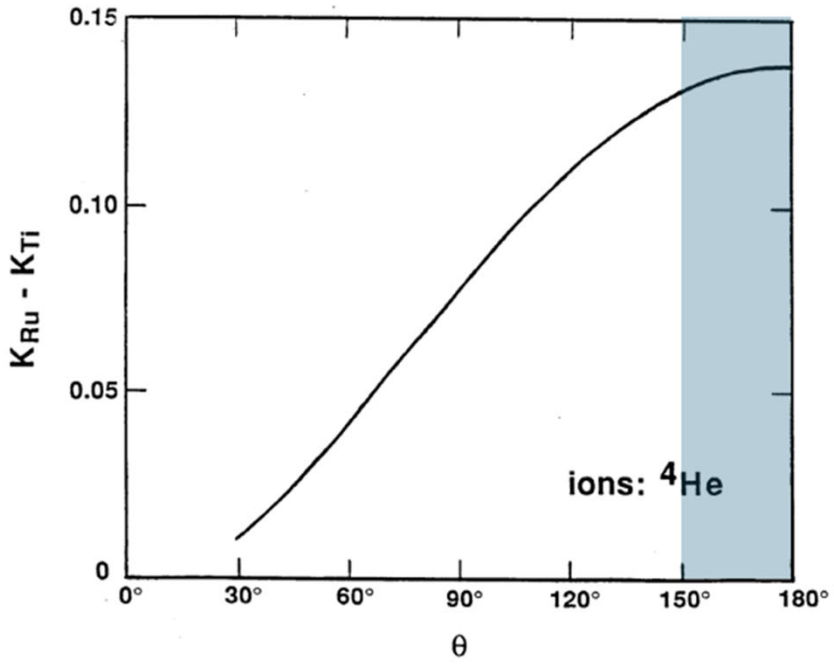

Mass separation: M_1 dependency

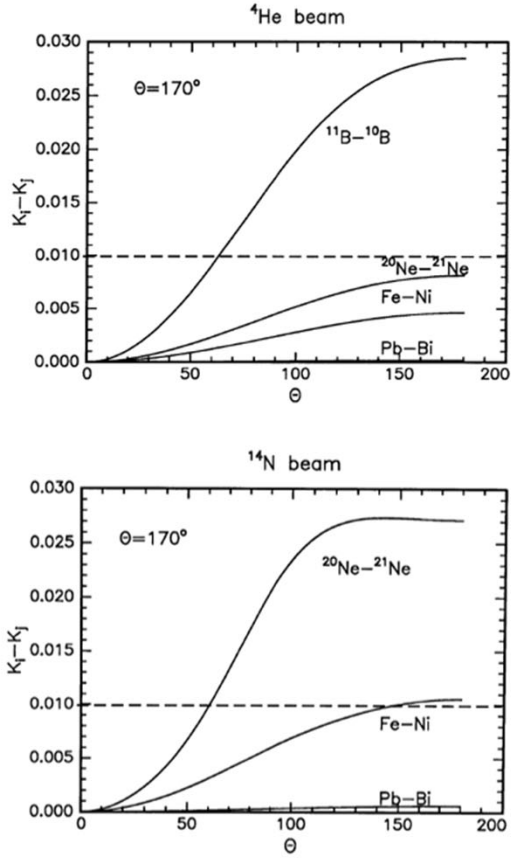

$$\Delta M_2 = \frac{\Delta E_d}{E_0 \dfrac{dK_{M_2}}{dM_2}}$$

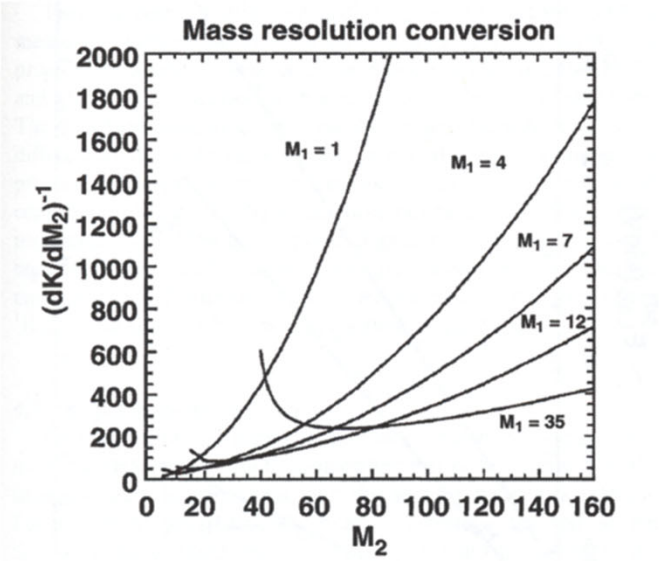

FIG. 4.2. Plots of $(dK/dM_2)^{-1}$ versus target mass M_2 for several analysis beams (M_1 = ion mass). Units of M_1 and M_2 are u. The laboratory backscattering angle is 180°. The plots can be used to estimate the mass resolution $\delta M_2 = (\delta E/E_0)\,(dK/dM_2)^{-1}$ if $\delta E/E_0$ is specified.

Handbook of Modern Ion Beam Materials Analysis (ISBN-10, 1605112151)

For distinguishing heavy atoms there might seem some advantage in using heavy ion beams, but.....

Mass separation: detector resolution dependency

$$\Delta M_2 = \frac{\Delta E_d}{E_0 \frac{dK_{M_2}}{dM_2}}$$

The energy resolution of the commonly and ubiquitously used silicon solid state detectors deteriorates rapidly with increasing Z_1, nullifying the effect of M_1.
Gas detectors MUST be used with ions heavier than Li.

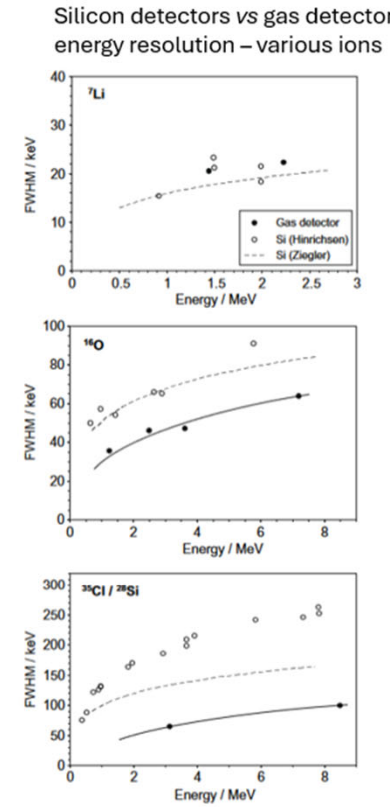

DOI: 10.1016/j.nimb.2009.01.031
DOI: 10.1016/S0168-583X(97)00664-2

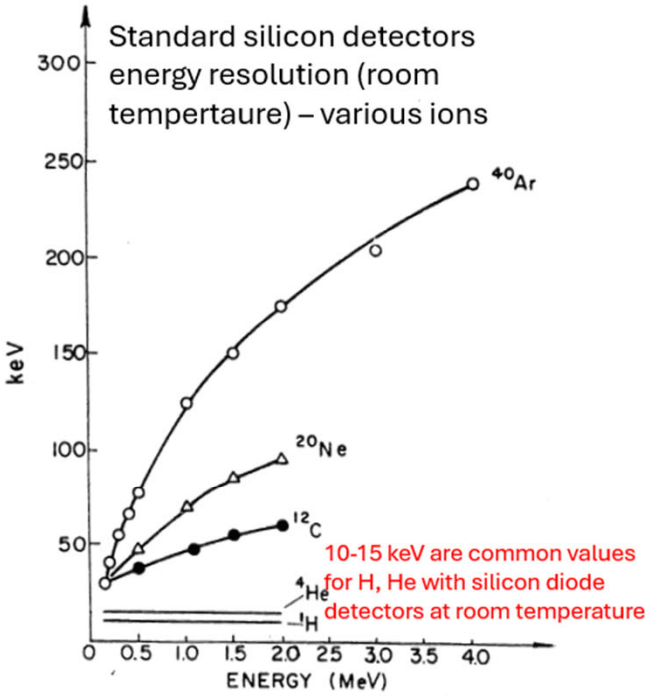

Taken from https://doi.org/10.1139/p68-635

In conclusion: typical conditions

- 1-2 MeV ^{4}He (or about 0.4-0.5 MeV ^{1}H) ions for Rutherford cross section use (2% error)
- silicon diode detectors (small, cheap, high efficiency)
- Backscattering angles in the range 150°-180° for highest mass separation

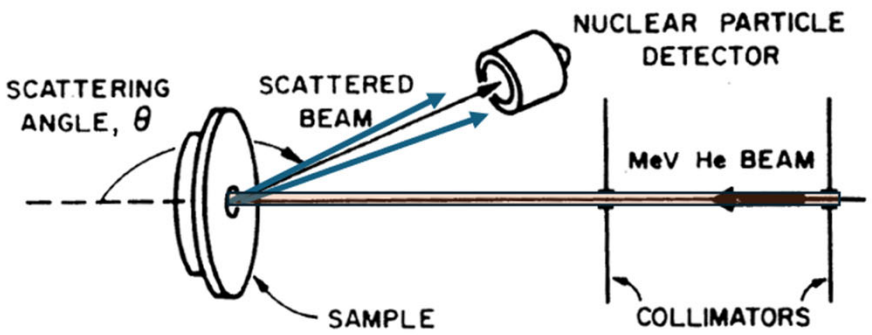

Θ=160°-170°

E_0=1.5-2.0 MeV

Beam: He+

Schematic of the experimental setup for Rutherford backscattering. A collimated beam of He ions is incident on a planar sample. Particles scattered to an angle θ are detected by a solid state nuclear particle detector. All this apparatus must be under vacuum.

$\sigma_{Rutherford}(\theta)$ @1 MeV (He+)

TABLE X. Rutherford Scattering Cross Section of the Elements for 1 MeV ^{4}He

ELEMENT	AT. NO. (Z_2)	AVRG MASS (amu)	$d\sigma/d\Omega$ (in 10^{-24} cm^2/steradian) 179.5°	170°	160°	150°	140°	130°	120°	110°	100°	90°
BE	4	9.012	0.05344	0.05458	0.05817	0.06467	0.075	0.09069	0.1143	0.1503	0.2065	0.2972
B	5	10.81	0.09648	0.09837	0.1043	0.1149	0.1316	0.1569	0.1945	0.2514	0.3395	0.4814
C	6	12.01	0.1474	0.1502	0.1588	0.1744	0.1988	0.2354	0.29	0.3722	0.4992	0.7036
N	7	14.01	0.2142	0.218	0.2299	0.2513	0.2849	0.3351	0.4098	0.522	0.6952	0.9734
O	8	16	0.2915	0.2965	0.3122	0.3403	0.3844	0.4503	0.548	0.6947	0.921	1.285
F	9	19	0.3834	0.3898	0.4097	0.4455	0.5014	0.585	0.7089	0.8948	1.181	1.641
NE	10	20.18	0.4783	0.4862	0.5109	0.5551	0.6242	0.7275	0.8805	1.11	1.464	2.032
NA	11	22.99	0.5897	0.5993	0.6291	0.6827	0.7664	0.8915	1.077	1.355	1.783	2.47
MG	12	24.31	0.7064	0.7178	0.7534	0.8172	0.9169	1.066	1.286	1.617	2.126	2.944
AL	13	26.98	0.8378	0.8512	0.893	0.9678	1.085	1.26	1.518	1.907	2.505	3.465
SI	14	28.09	0.975	0.9905	1.039	1.126	1.262	1.464	1.765	2.215	2.908	4.022
P	15	30.97	1.127	1.145	1.201	1.301	1.457	1.689	2.034	2.551	3.347	4.625
S	16	32.06	1.286	1.306	1.369	1.483	1.66	1.925	2.317	2.905	3.811	5.265
CL	17	35.45	1.46	1.483	1.554	1.683	1.883	2.182	2.624	3.288	4.311	5.953
AR	18	39.95	1.646	1.671	1.752	1.895	2.12	2.455	2.951	3.696	4.842	6.683
K	19	39.1	1.832	1.861	1.95	2.11	2.36	2.734	3.287	4.116	5.394	7.444
CA	20	40.08	2.032	2.064	2.163	2.34	2.617	3.031	3.644	4.563	5.978	8.251
SC	21	44.96	2.249	2.285	2.394	2.589	2.895	3.351	4.027	5.04	6.601	9.106
TI	22	47.9	2.474	2.512	2.632	2.846	3.182	3.683	4.424	5.536	7.249	9.998
V	23	50.94	2.708	2.75	2.881	3.116	3.482	4.03	4.84	6.055	7.927	10.93
CR	24	52	2.95	2.996	3.138	3.394	3.793	4.389	5.271	6.594	8.633	11.91
MN	25	54.94	3.205	3.255	3.409	3.687	4.12	4.766	5.724	7.159	9.372	12.92
FE	26	55.85	3.468	3.521	3.689	3.989	4.457	5.157	6.192	7.745	10.14	13.98
CO	27	58.93	3.743	3.801	3.982	4.305	4.811	5.565	6.682	8.356	10.94	15.08
NI	28	58.71	4.026	4.088	4.282	4.63	5.173	5.984	7.185	8.986	11.76	16.21
CU	29	63.54	4.324	4.391	4.599	4.972	5.555	6.425	7.714	9.645	12.62	17.4
ZN	30	65.37	4.63	4.701	4.924	5.323	5.947	6.878	8.257	10.32	13.51	18.62
GA	31	69.72	4.948	5.024	5.262	5.688	6.355	7.349	8.821	11.03	14.43	19.89
GE	32	72.59	5.275	5.356	5.61	6.064	6.774	7.833	9.402	11.75	15.38	21.2
AS	33	74.92	5.612	5.698	5.968	6.451	7.206	8.333	10	12.5	16.36	22.54
SE	34	78.96	5.96	6.052	6.339	6.851	7.653	8.849	10.62	13.27	17.37	23.93
BR	35	79.91	6.317	6.414	6.718	7.261	8.11	9.378	11.25	14.07	18.4	25.36
KR	36	83.8	6.686	6.789	7.11	7.685	8.583	9.924	11.91	14.89	19.47	26.84
RB	37	85.47	7.064	7.173	7.512	8.119	9.068	10.48	12.58	15.73	20.57	28.35
SR	38	87.62	7.453	7.567	7.925	8.565	9.566	11.06	13.27	16.59	21.7	29.9
Y	39	88.91	7.851	7.972	8.348	9.023	10.08	11.65	13.98	17.47	22.86	31.5
ZR	40	91.22	8.26	8.388	8.784	9.494	10.6	12.26	14.71	18.38	24.05	33.14
NB	41	92.91	8.68	8.813	9.23	9.975	11.14	12.88	15.46	19.32	25.27	34.81
MO	42	95.94	9.11	9.251	9.687	10.47	11.69	13.52	16.22	20.27	26.52	36.54
TC	43	99	9.552	9.698	10.16	10.98	12.26	14.17	17	21.25	27.8	38.3
RU	44	101.1	10	10.16	10.64	11.49	12.84	14.84	17.81	22.25	29.1	40.1
RH	45	102.9	10.46	10.62	11.13	12.02	13.43	15.52	18.63	23.28	30.44	41.95
PD	46	106.4	10.94	11.1	11.63	12.57	14.03	16.22	19.46	24.32	31.81	43.83
AG	47	107.9	11.42	11.59	12.14	13.12	14.65	16.94	20.32	25.39	33.21	45.76

$\sigma_{Rutherford}(\theta)$ @1 MeV (He+)

CD	48	112.4	11.91	12.09	12.66	13.69	15.28	17.67	21.2	26.49	34.64	47.73
IN	49	114.8	12.41	12.6	13.2	14.26	15.93	18.41	22.09	27.61	36.1	49.74
SN	50	118.7	12.93	13.13	13.74	14.85	16.59	19.17	23	28.75	37.59	51.8
SB	51	121.8	13.45	13.66	14.3	15.46	17.26	19.95	23.93	29.91	39.11	53.89
TE	52	127.6	13.99	14.2	14.87	16.07	17.94	20.74	24.89	31.1	40.67	56.03
I	53	126.9	14.53	14.75	15.45	16.69	18.64	21.55	25.85	32.3	42.25	58.2
XE	54	131.3	15.08	15.32	16.04	17.33	19.35	22.37	26.84	33.54	43.86	60.42
CS	55	132.9	15.65	15.89	16.64	17.98	20.08	23.21	27.84	34.79	45.5	62.68
BA	56	137.3	16.23	16.47	17.25	18.64	20.82	24.06	28.87	36.07	47.17	64.98
LA	57	138.9	16.81	17.07	17.87	19.31	21.57	24.93	29.91	37.37	48.87	67.32
CE	58	140.1	17.41	17.67	18.51	20	22.33	25.81	30.97	38.69	50.6	69.71
PR	59	140.9	18.01	18.29	19.15	20.69	23.11	26.71	32.04	40.04	52.36	72.13
ND	60	144.2	18.63	18.91	19.81	21.4	23.9	27.62	33.14	41.41	54.15	74.6
PM	61	147	19.26	19.55	20.47	22.12	24.7	28.55	34.25	42.8	55.97	77.11
SM	62	150.4	19.89	20.2	21.15	22.86	25.52	29.5	35.39	44.22	57.82	79.66
EU	63	152	20.54	20.86	21.84	23.6	26.35	30.46	36.54	45.66	59.7	82.25
GD	64	157.3	21.2	21.53	22.54	24.36	27.2	31.44	37.71	47.12	61.62	84.88
TB	65	158.9	21.87	22.2	23.25	25.13	28.05	32.43	38.9	48.6	63.56	87.56
DY	66	162.5	22.55	22.89	23.97	25.91	28.92	33.43	40.11	50.11	65.53	90.27
HO	67	164.9	23.24	23.59	24.71	26.7	29.81	34.45	41.33	51.64	67.53	93.03
ER	68	167.3	23.94	24.3	25.45	27.5	30.71	35.49	42.58	53.2	69.56	95.83
TM	69	168.9	24.65	25.03	26.2	28.32	31.62	36.54	43.84	54.77	71.62	98.67
YB	70	173	25.37	25.76	26.97	29.14	32.54	37.61	45.12	56.37	73.72	101.5
LU	71	175	26.1	26.5	27.75	29.98	33.48	38.69	46.42	58	75.84	104.5
HF	72	178.5	26.84	27.25	28.54	30.84	34.43	39.79	47.73	59.64	77.99	107.4
TA	73	181	27.59	28.01	29.33	31.7	35.39	40.91	49.07	61.31	80.17	110.4
W	74	183.9	28.35	28.79	30.14	32.57	36.37	42.04	50.43	63	82.38	113.5
RE	75	186.2	29.13	29.57	30.97	33.46	37.36	43.18	51.8	64.72	84.63	116.6
OS	76	190.2	29.91	30.37	31.8	34.36	38.36	44.34	53.19	66.46	86.9	119.7
IR	77	192.2	30.7	31.17	32.64	35.27	39.38	45.52	54.6	68.22	89.2	122.9
PT	78	195.1	31.5	31.99	33.49	36.19	40.41	46.71	56.03	70	91.53	126.1
AU	79	197	32.32	32.81	34.36	37.13	41.45	47.91	57.47	71.81	93.9	129.3
HG	80	200.6	33.14	33.65	35.24	38.08	42.51	49.13	58.94	73.64	96.29	132.6
TL	81	204.4	33.98	34.5	36.12	39.03	43.58	50.37	60.42	75.49	98.71	136
PB	82	207.2	34.82	35.36	37.02	40	44.67	51.62	61.92	77.37	101.2	139.4
BI	83	209	35.68	36.22	37.93	40.99	45.76	52.89	63.44	79.27	103.7	142.8
PO	84	210	36.54	37.1	38.85	41.98	46.87	54.17	64.98	81.19	106.2	146.2
AT	85	210	37.42	37.99	39.78	42.99	47.99	55.47	66.54	83.13	108.7	149.7
RN	86	222	38.31	38.89	40.73	44.01	49.13	56.79	68.12	85.1	111.3	153.3
FR	87	223	39.2	39.8	41.68	45.04	50.28	58.11	69.71	87.1	113.9	156.9
RA	88	226	40.11	40.72	42.64	46.08	51.45	59.46	71.32	89.11	116.5	160.5
AC	89	227	41.03	41.66	43.62	47.13	52.62	60.82	72.95	91.15	119.2	164.2
TH	90	232	41.95	42.6	44.6	48.2	53.81	62.19	74.6	93.21	121.9	167.9
PA	91	231	42.89	43.55	45.6	49.27	55.01	63.58	76.27	95.29	124.6	171.6
U	92	238	43.84	44.51	46.61	50.36	56.23	64.99	77.96	97.4	127.4	175.4

For a thin target of thickness Δt with N atoms/cm^3 the YIELD, or the number of detected backscattered particles in a detector, that subtends a solid angle Ω around the angle θ, is:

$$\boldsymbol{Y} = \sigma(E,\theta)\Omega Q N \Delta t/\cos(\alpha)$$

Q= total number of incident particles in the beam
α= angle between beam direction and sample normal (α= 0 for normal incidence)

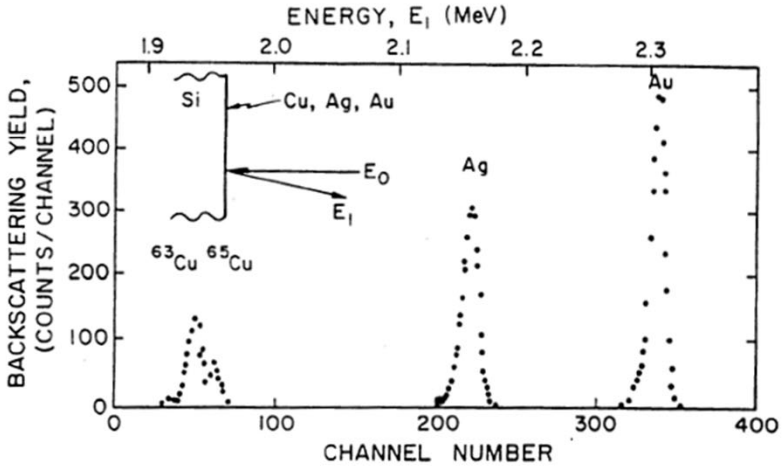

Example

2.0 MeV, He$^+$, θ =170°, α=0, on a 10^{15} at/cm^2 gold contamination at surface.
Charge=10 μC, Ω =1 msr.

$$Y_{Au} = 32.81\ 10^{-24} * 0.001 * 10 * 10^{-6} * 6.2415\ 10^{18} * 10^{15}$$

σ ($\frac{barn}{sr}$) Ω (sr) Q (μC) NΔt (at/cm^2)

~2000 counts

Absolute coverages of a heavy element on a light substrate can be detected down to a limit of **10^{-3} monolayers**

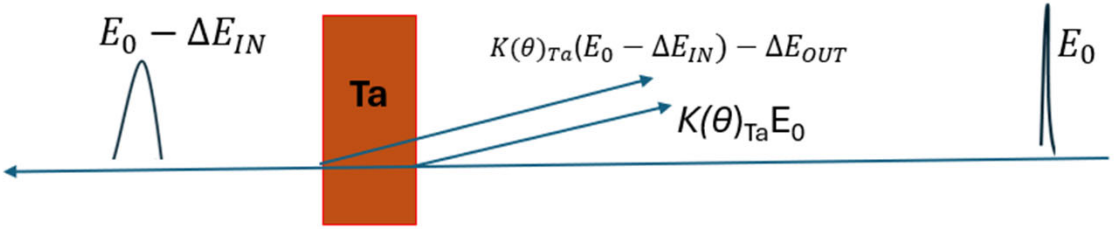
$E_0 - \Delta E_{IN}$
Ta
$K(\theta)_{Ta}(E_0 - \Delta E_{IN}) - \Delta E_{OUT}$
$K(\theta)_{Ta}E_0$
E_0

$N\Delta t_{Ta}$

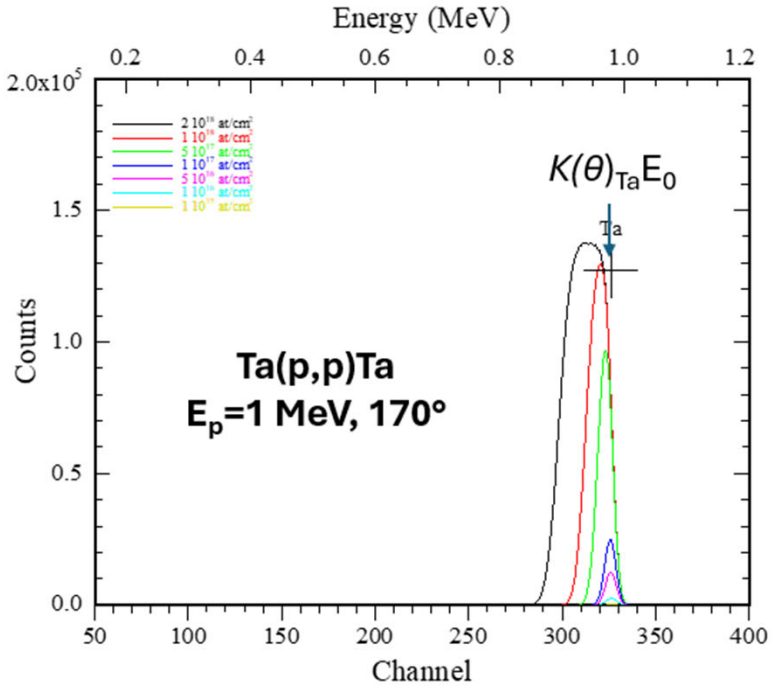
Energy (MeV)
Counts
Channel
$K(\theta)_{Ta}E_0$
Ta
Ta(p,p)Ta
E_p=1 MeV, 170°

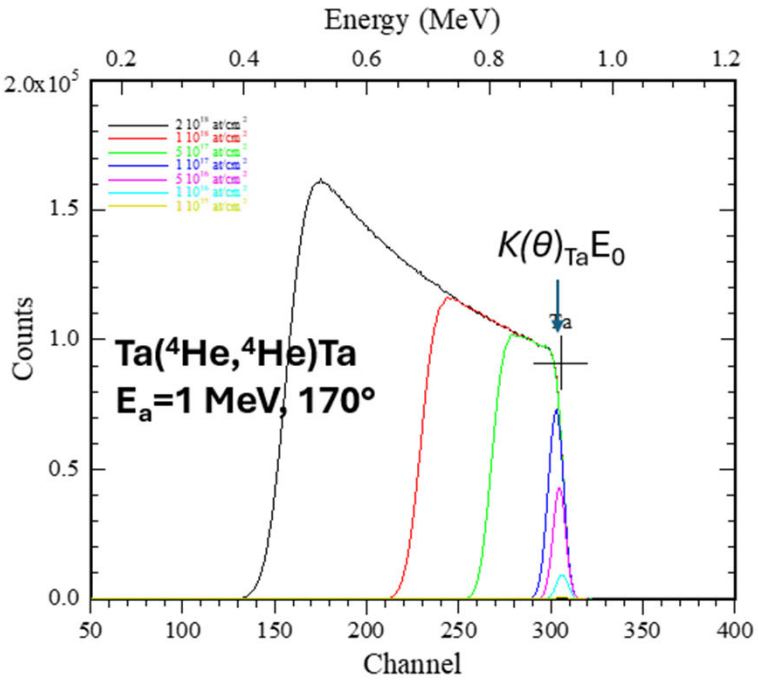
Energy (MeV)
Counts
Channel
$K(\theta)_{Ta}E_0$
Ta
Ta(^{4}He,^{4}He)Ta
E_a=1 MeV, 170°

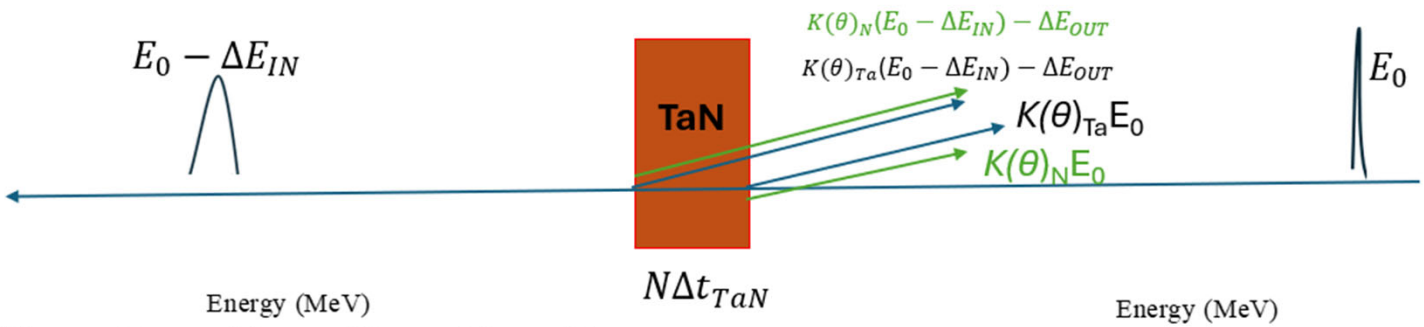
$E_0 - \Delta E_{IN}$
TaN
$K(\theta)_N(E_0 - \Delta E_{IN}) - \Delta E_{OUT}$
$K(\theta)_{Ta}(E_0 - \Delta E_{IN}) - \Delta E_{OUT}$
$K(\theta)_{Ta}E_0$
$K(\theta)_N E_0$
E_0
$N\Delta t_{TaN}$

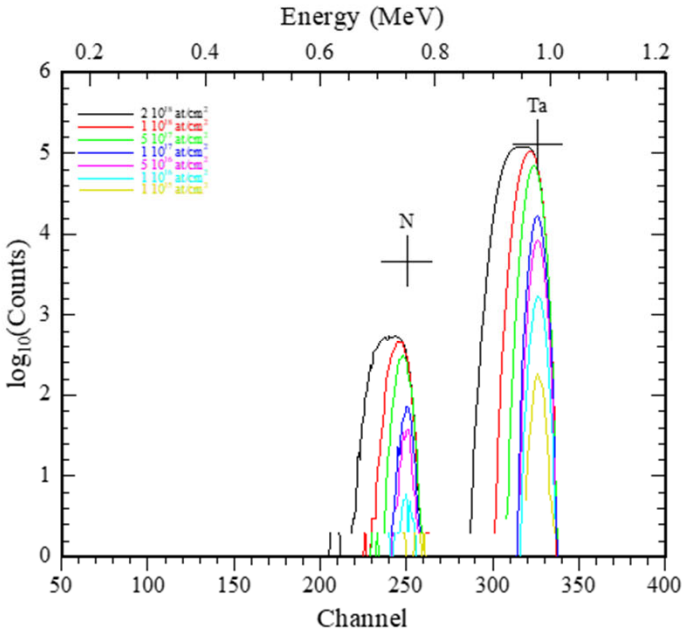
Energy (MeV)
0.2
0.4
0.6
0.8
1.0
1.2
Ta
N
log10(Counts)
Channel
50
100
150
200
250
300
350
400

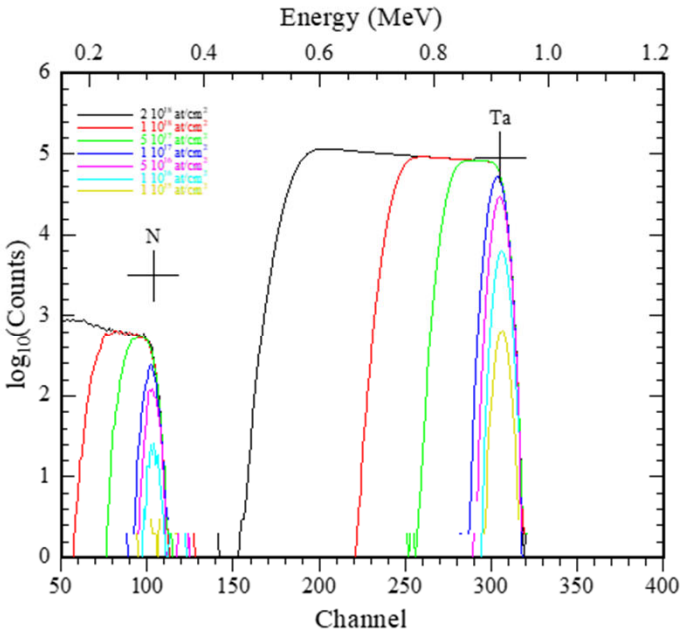
Energy (MeV)
0.2
0.4
0.6
0.8
1.0
1.2
Ta
N
log10(Counts)
Channel
50
100
150
200
250
300
350
400

Energy loss and stopping cross section

The amount of energy ΔE lost per distance Δt (cm) traversed by the ion, depends on the identity of projectile, on the density N *(at/cm³)* and composition of the target and on the energy E_0 of the projectile. In scattering experiments the thickness Δa is measured in atoms/cm²:

$$\Delta a = N\Delta t$$

The energy difference ΔE of the particles before and after transmission through the target can be measured accurately. The energy loss per unit lenght dE/da at the energy E_0 of the incident beam is defined as

$$\lim_{\Delta a \to 0} \frac{\Delta E}{\Delta a} = \frac{dE}{da}(E_0)$$

and is called 'stopping cross section' and is typically measured in eV/(10^{15}at/cm²).

For a compound A_nB_m (with n+m=1) the stopping cross section is given as

$$n\frac{dE^A}{da}(E_0) + m\frac{dE^B}{da}(E_0)$$

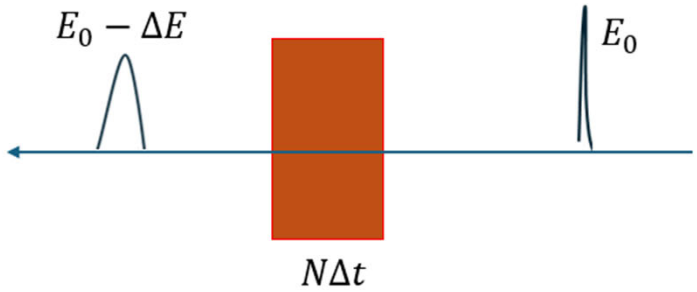

The stopping cross section has been measured for most solid elements, gas and for many compounds, for He and H ions, in a wide range of energies. Models have been proposed and tested and several databases with experimental data are available.
See: http://srim.org
(collects stopping data from more than 2300 papers)

Energy loss and stopping cross section

Calculation of stopping cross section of compound TaN, from individual stopping curves of Ta and nitrogen.

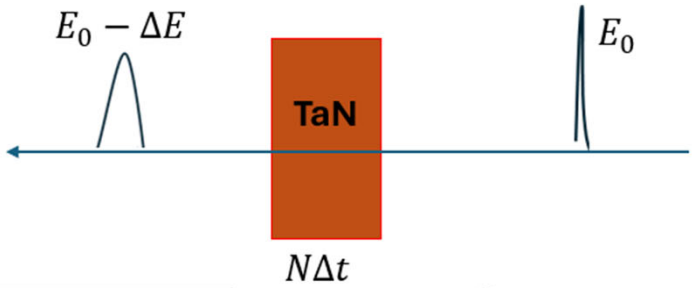

Uncertainty in stopping cross section calculation varies from 4% to about 10-20%

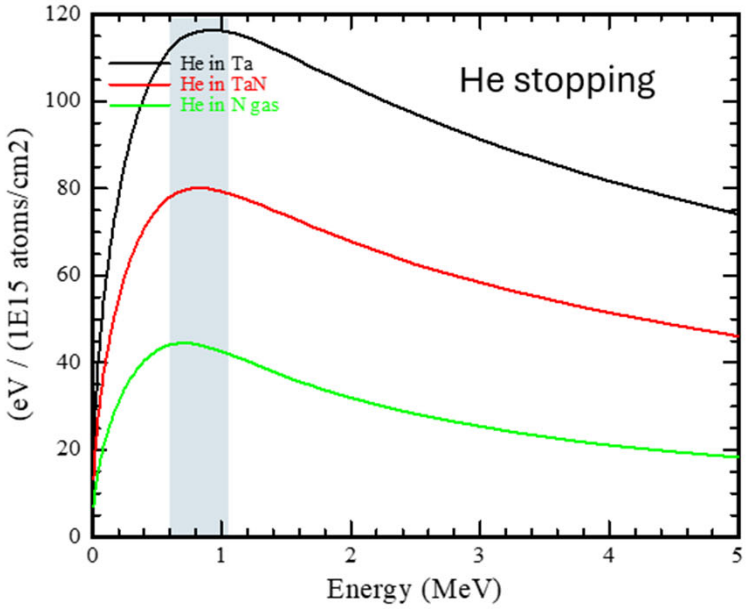

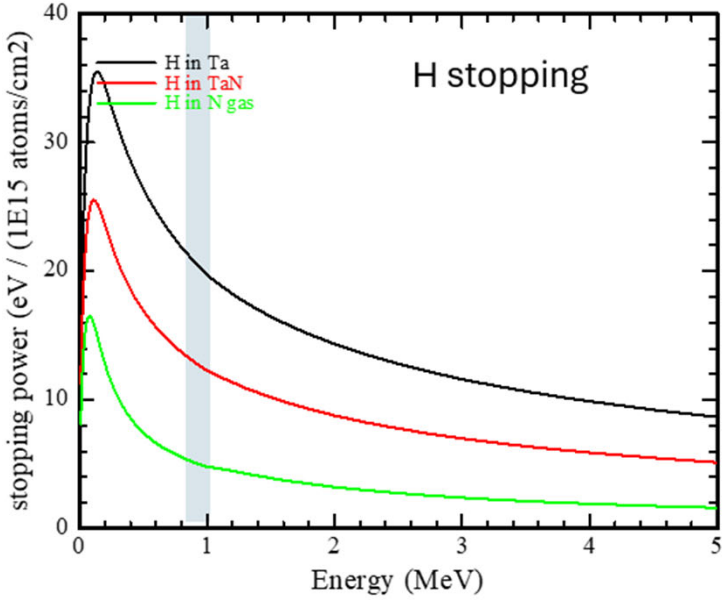

http://srim.org/

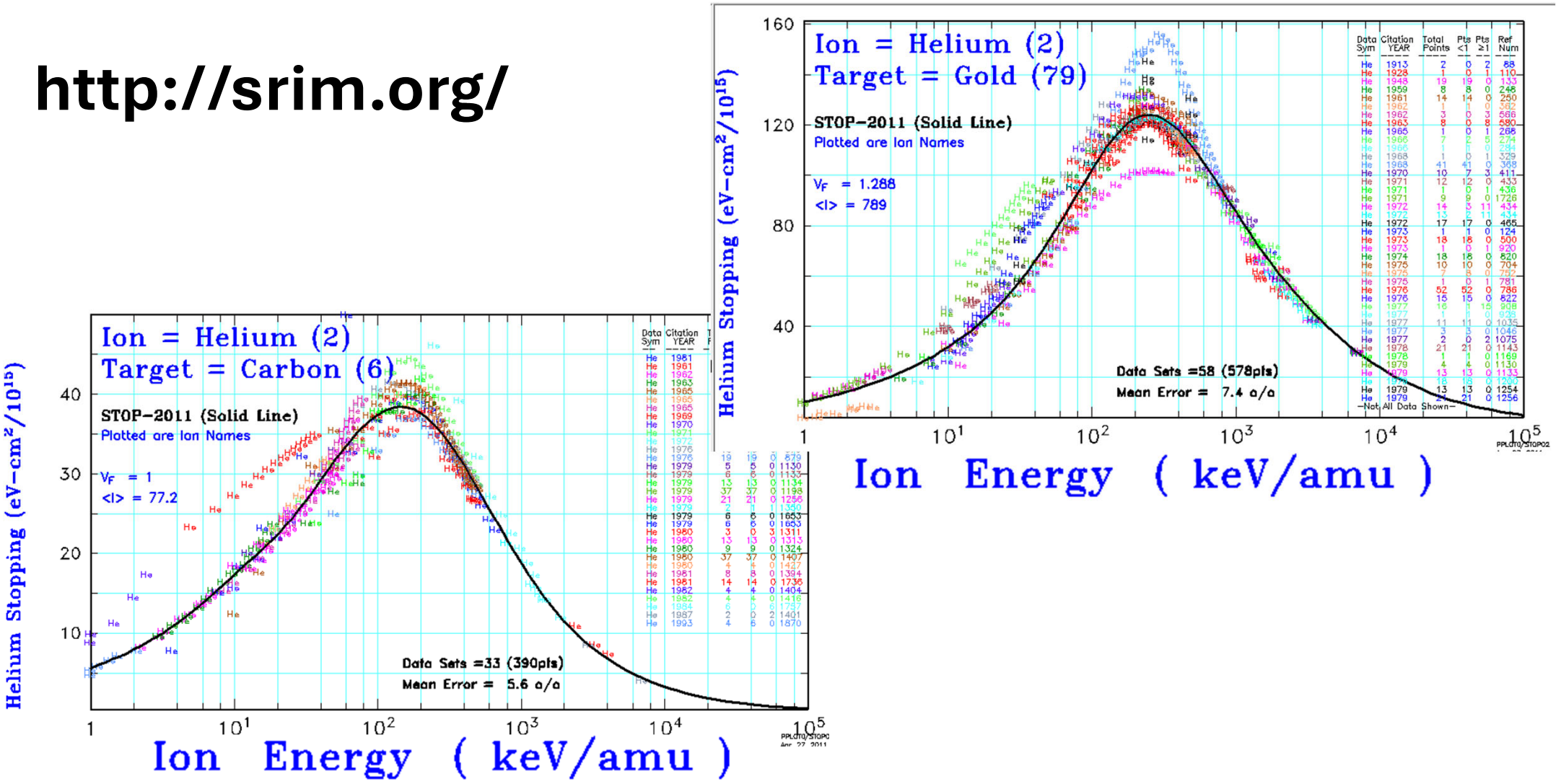

Stopping cross section and the depth scale

The stopping cross section curves can be used to correlate the energy lost by the probing ion, $\Delta E = E - E_0$, to the thickness penetrated in target material $\Delta a = N\Delta t/\cos(\alpha)$.

The calculation involves solving integrals such as:

$$\Delta E = \boldsymbol{E}(\Delta a) - E_0 = -\int_0^{\Delta a} \frac{dE(\boldsymbol{E}(x), x)}{dx} dx$$

$$\Delta a(E) = \int_E^{E_0} \left(\frac{dE}{da}(E)\right)^{-1} dE$$

which give, through iterations, the desired energy-depth relation.

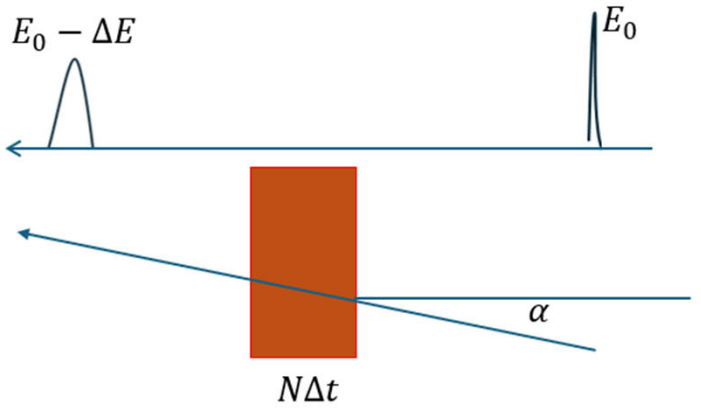

Depth resolution and energy straggling

The depth resolution $\delta a_\perp$ (measured normally to the surface) is the capability of the probe ion to resolve details (such as variation of composition, layered structured, buried layers...) in depth, during the slowing down into the material.
It is expressed as

$$\delta a_\perp \propto \cos(\alpha) \frac{\sqrt{(\Delta E_d)^2+(\Delta E_s)^2+(\Delta E_{beam})^2}}{\left(\frac{dE}{da}\right)}$$

ΔE_d = detector resolution
ΔE_s = energy straggling due to energy loss fluctuation
ΔE_{beam} = beam energy spread

ΔE_i^2 are the variances of the relative energy distribution functions. The sum of the variances gives the total energy resolution as a function of depth (energy).

The depth resolution $\delta a_\perp$ improves if

- α increases: for smooth samples $0 \leq \alpha \leq 75°$
- The stopping power increases: He better than H
- Detector has very good resolution
- Beam has low energy spread

- Energy straggling is low (near surface scattering, see next)

Energy loss straggling

The $(\Delta E_s)^2$ term originates from the fact that an energetic particle moving through a medium loses energy via many individual encounters. Such a discrete process is subject to statistical fluctuations. As a result, the energy loss ΔE is subject to fluctuations around its mean value (related to the stopping power). This phenomenon is called 'energy loss straggling' or simply 'energy straggling' and represents the variance of the energy distribution of the particle as a function of travelled path X.
For MeV He or H ions a good approximation is given by the Bohr's formula

$$\Omega^2_{Bohr} = (\Delta E_s)^2 = 4\pi(Z_1 e^2)^2 Z_2 N \Delta x$$

Clearly, for scattering at the surface ΔE_s=0

Bohr's treatment has been improved by many authors to extend the applicability to lower energy and heavy ions.
(DOI:https://doi.org/10.1103/PhysRevA.49.1089)

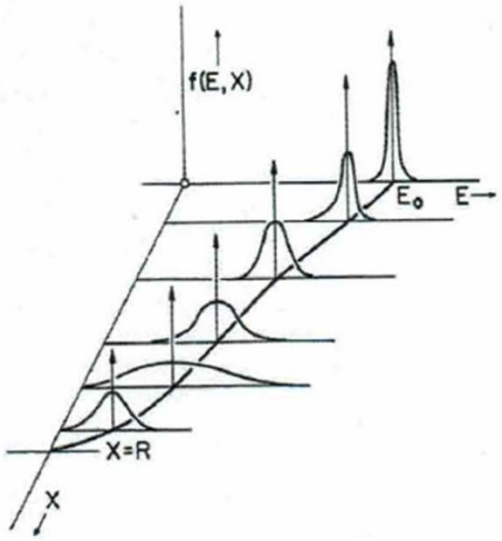

Evolution of the energy distribution as a function of depth as the ion traverses a material. The energy spread due to straggling increases with depth until the lowest-energy ions of the beam reach the energy of the maximum stopping. Below this energy, the energy loss decreases with decreasing energy leading to a sort of bunching of the straggling distribution.

Handbook of Modern Ion Beam Materials Analysis (ISBN-10, 1605112151)

Additivity of energy straggling

Considering two elements A, B, with atomic densities N^A, N^B and atomic number Z_A , Z_B we deduce from the Bohr's formula:

$$\frac{\left(\Omega^A_{Bohr}\right)^2}{N^A Z_A \Delta x} = \frac{\left(\Omega^B_{Bohr}\right)^2}{N^B Z_B \Delta x} = 4\pi(Z_1 e^2)^2$$

In a compound (mixture) A_mC_n, with m+n=1 and density $N^{A_mB_n}$

$$\frac{\left(\Omega^{A_mB_n}_{Bohr}\right)^2}{\begin{pmatrix} number\ of\ electrons\ per\ unit\ area \\ of\ the\ target\ of\ thickness\ \Delta x \end{pmatrix}} = \frac{\left(\Omega^{A_mB_n}_{Bohr}\right)^2}{(mZ_A + nZ_B)\, N^{A_mB_n} \Delta x} = 4\pi(Z_1 e^2)^2$$

Energy straggling calculation in EBS

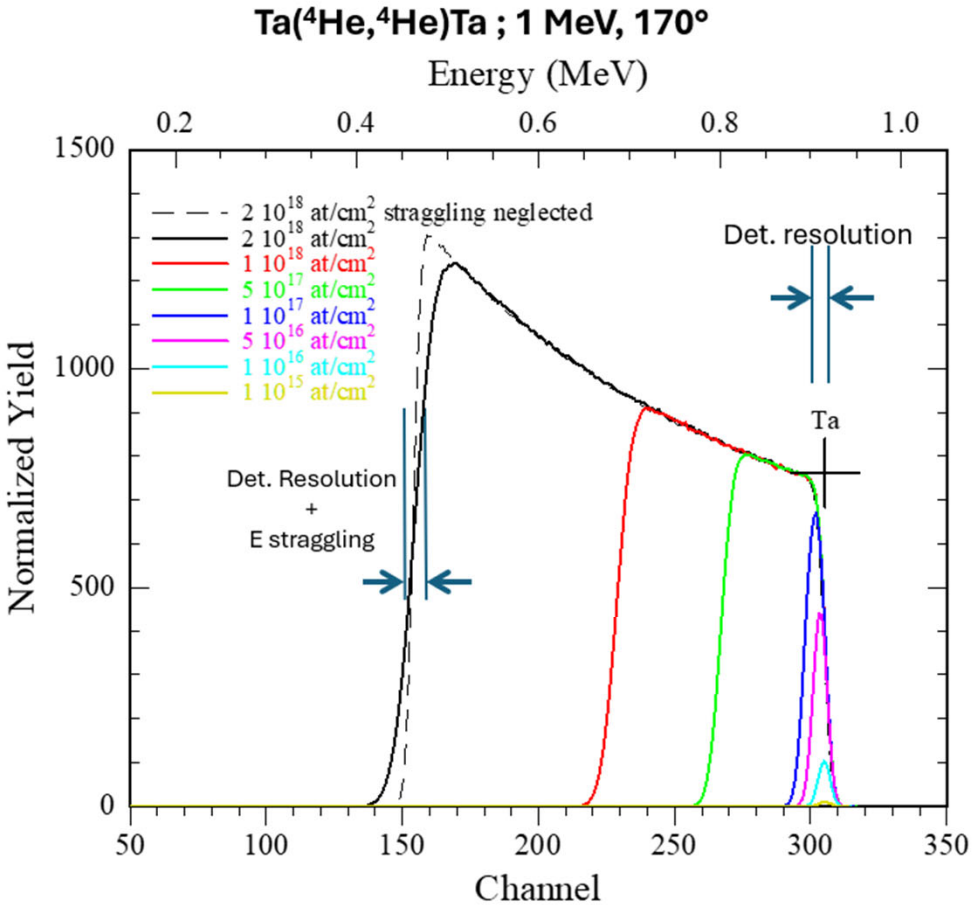

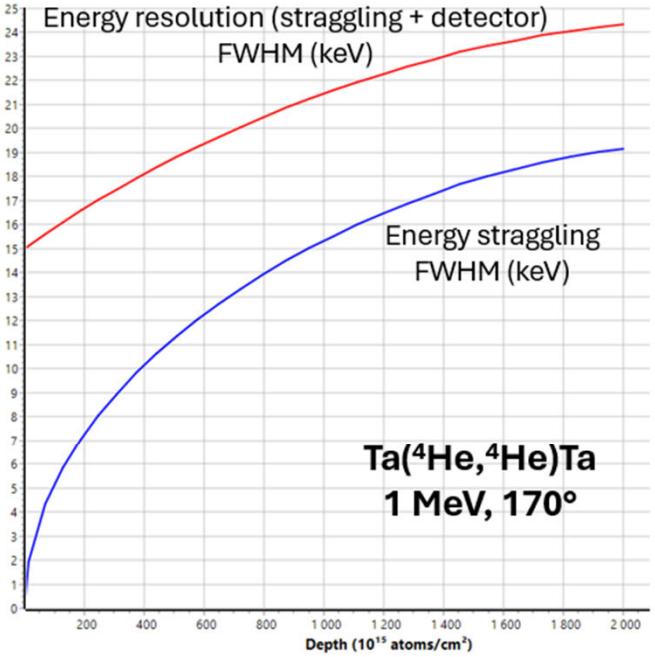

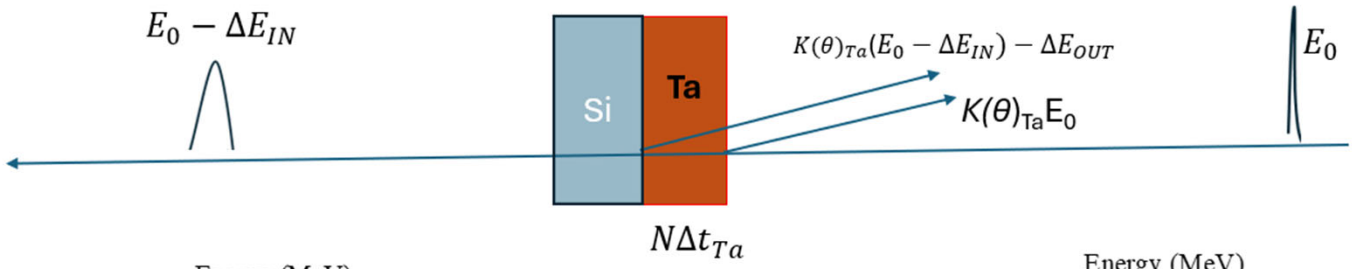
$E_0 - \Delta E_{IN}$
Si
Ta
$K(\theta)_{Ta}(E_0 - \Delta E_{IN}) - \Delta E_{OUT}$
$K(\theta)_{Ta}E_0$
E_0
$N\Delta t_{Ta}$

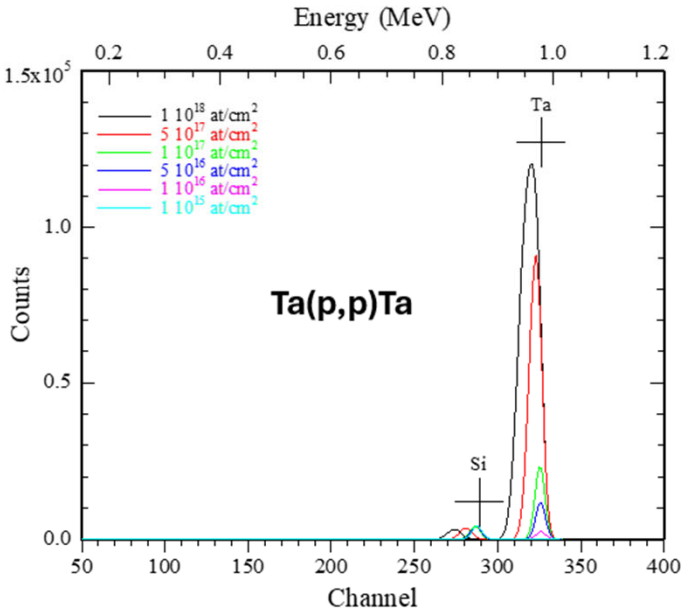
Energy (MeV)
0.2
0.4
0.6
0.8
1.0
1.2
1.5x10^5
1.0
0.5
0.0
Counts
1 10^18 at/cm^2
5 10^17 at/cm^2
1 10^17 at/cm^2
5 10^16 at/cm^2
1 10^16 at/cm^2
1 10^15 at/cm^2
Ta(p,p)Ta
Ta
Si
50
100
150
200
250
300
350
400
Channel

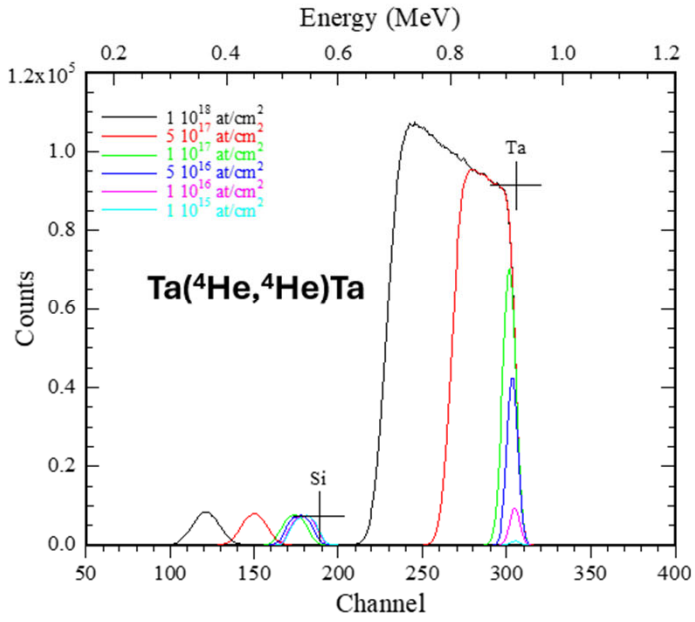
Energy (MeV)
0.2
0.4
0.6
0.8
1.0
1.2
1.2x10^5
1.0
0.8
0.6
0.4
0.2
0.0
Counts
1 10^18 at/cm^2
5 10^17 at/cm^2
1 10^17 at/cm^2
5 10^16 at/cm^2
1 10^16 at/cm^2
1 10^15 at/cm^2
Ta(⁴He,⁴He)Ta
Ta
Si
50
100
150
200
250
300
350
400
Channel

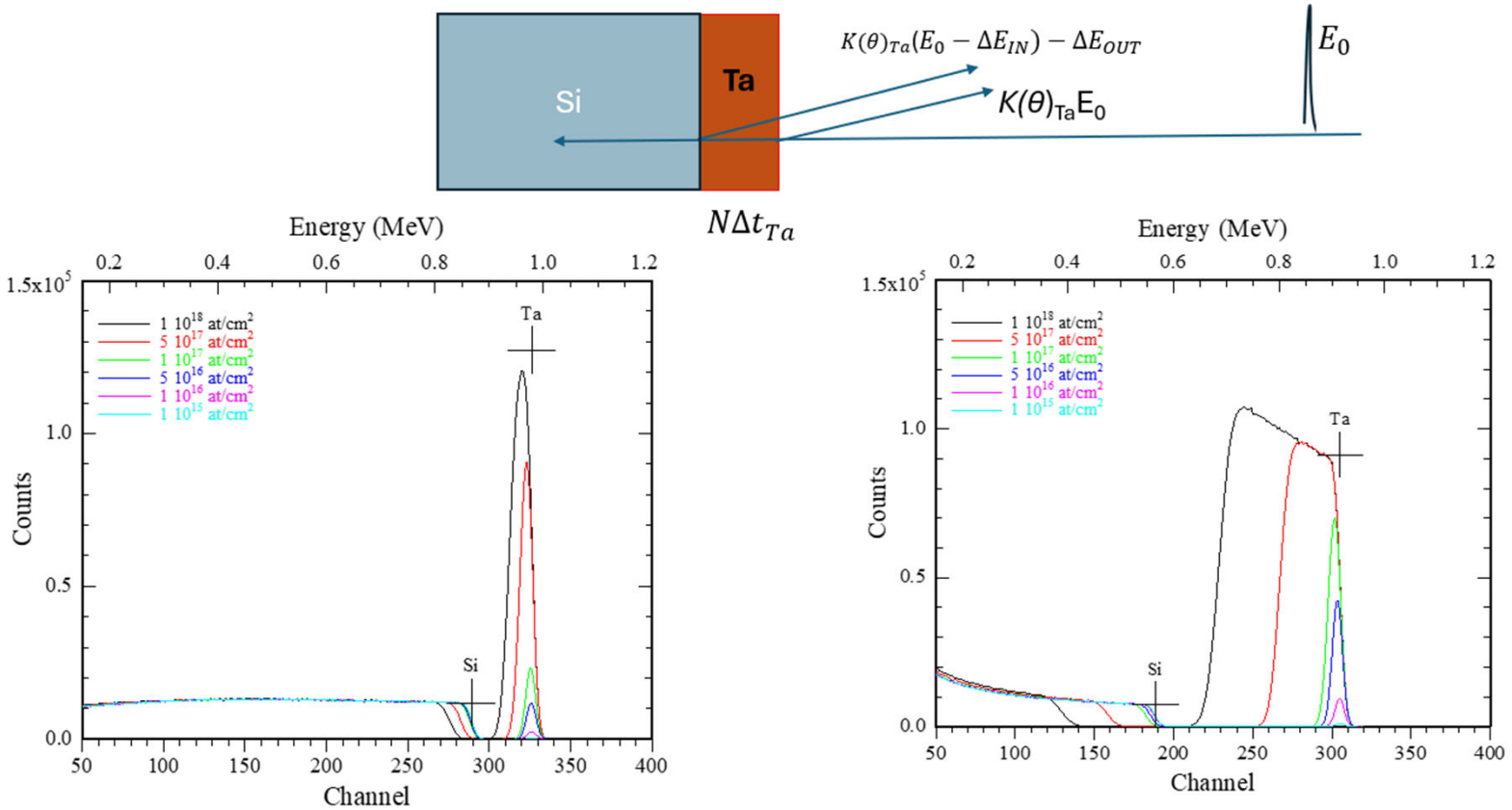
Si
Ta
$K(\theta)_{Ta}(E_0 - \Delta E_{IN}) - \Delta E_{OUT}$
$K(\theta)_{Ta}E_0$
E_0
$N\Delta t_{Ta}$
Energy (MeV)
Counts
Channel
Ta
Si
1 10^18 at/cm^2
5 10^17 at/cm^2
1 10^17 at/cm^2
5 10^16 at/cm^2
1 10^16 at/cm^2
1 10^15 at/cm^2

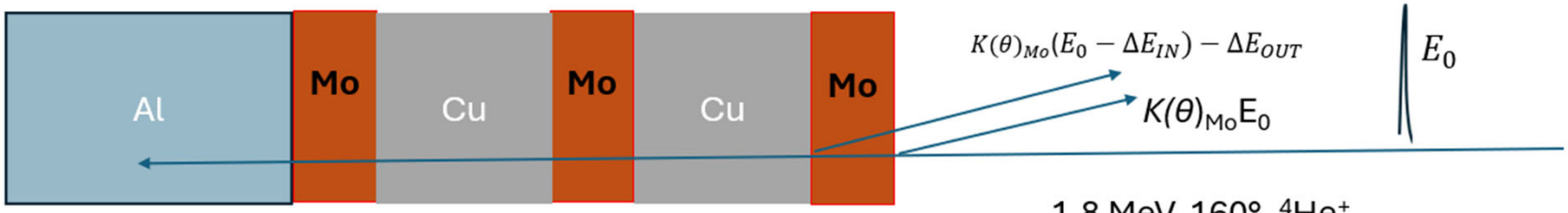

1.8 MeV, 160°, $^4He^+$
Microprobe (μRBS)
Beam size: 20 μm

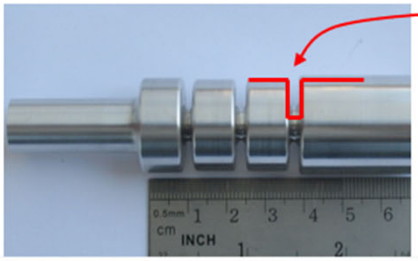

Mo/Cu metallic nano-layers deposited by ionized sputtering inside a trench with aspect ratio = 5.

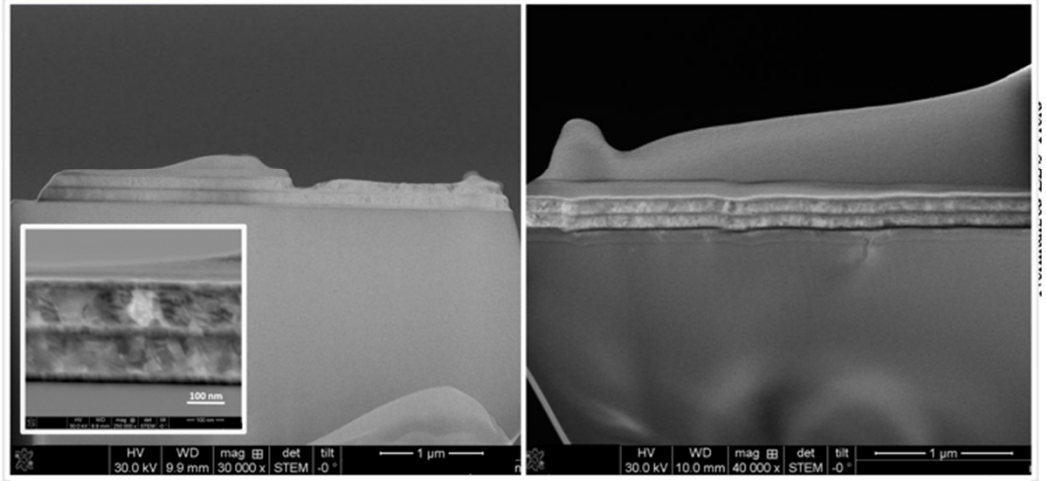

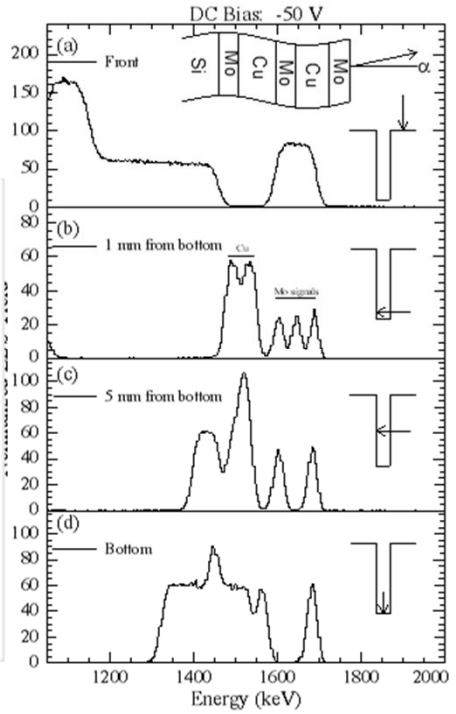

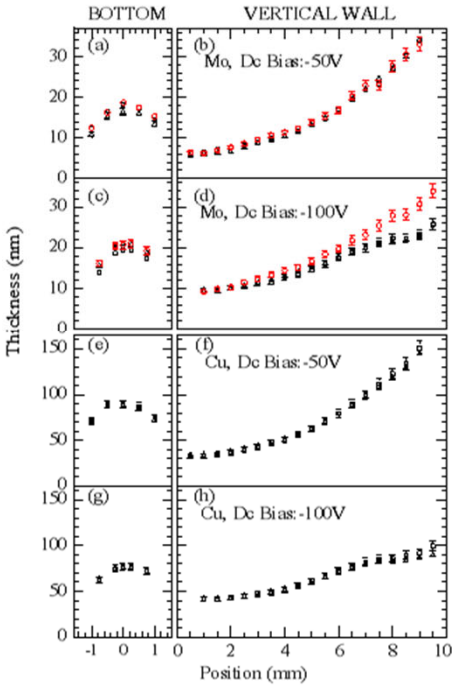

Example of μ**RBS** 2-D maps using μ-beams

Tantalum (6.9 µm) coating deposited onto copper is continuously irradiated with He+ ions (1.5 MeV).

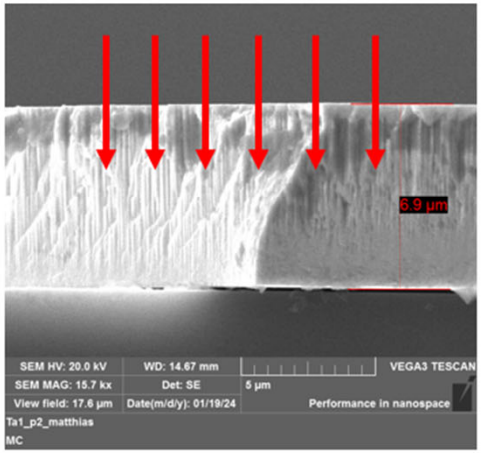

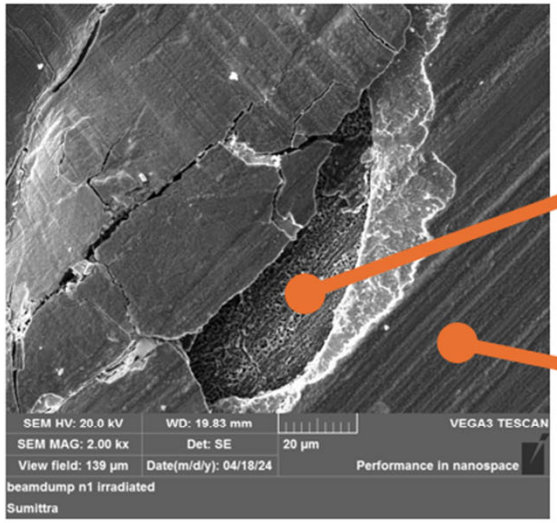

He bubbles are created at a depth of about 2.4 µm and cause surface blisters.

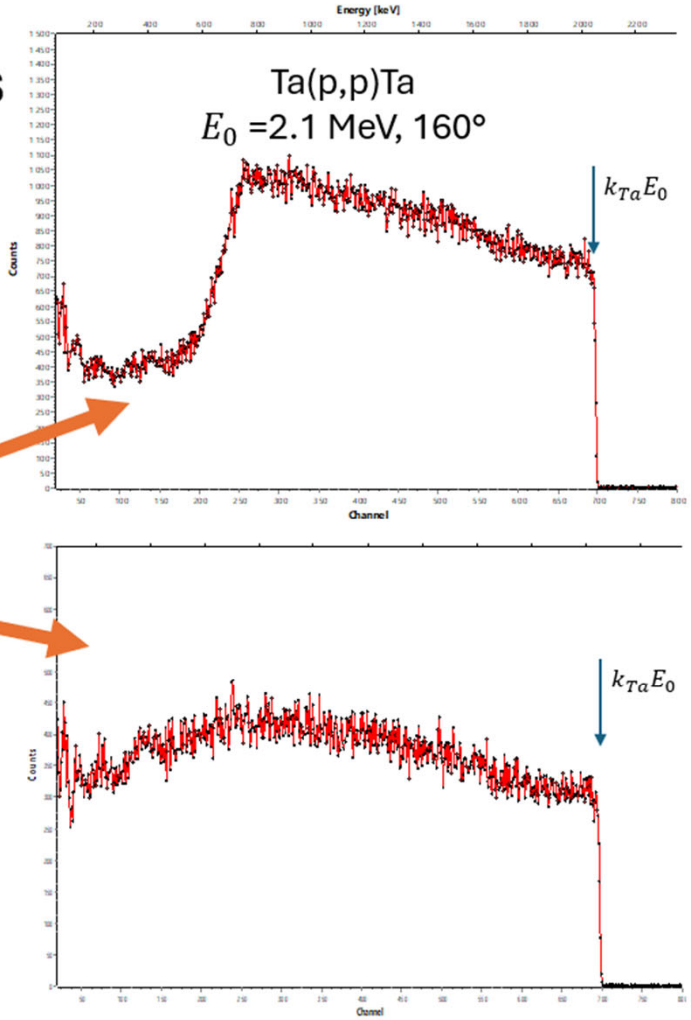

LNL AN2000 accelerator micro-probe apparatus

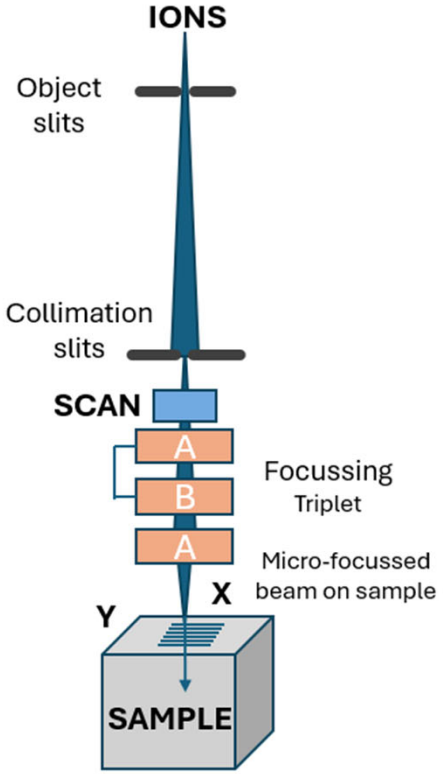

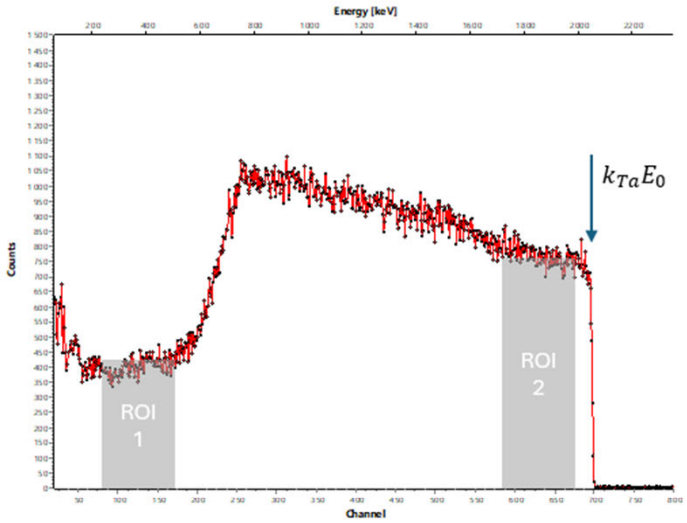

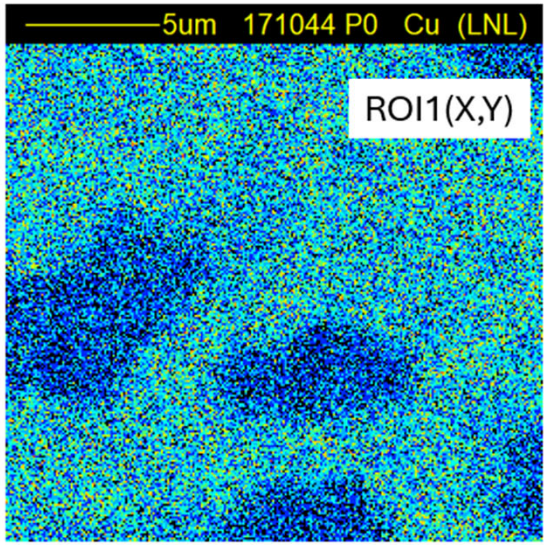

The backscattered protons in spectral region ROI1 are put in coincidence with the X,Y beam position of the micro-focussed (about **5 µm**) proton beam.

Once the map is completed µEBS spectra can be collected inside and ouside the delaminated regions to determine how much material (Ta) is still in place.

Elastic (non-Rutherford) backscattering cross section (I)

- Complex and sometimes large deviations (resonances) from the Rutherford value of the elastic scattering cross sections are observed for ^{1}H and ^{4}He ions, as a consequence of nuclear interaction (after tunneling through the Coulomb barrier) particularly in low atomic number target elements/isotopes, starting from some hundreds keV.

- An example is given by astrophysics studies of nuclear capture reactions (p,γ) at stellar temperatures (a few tens keV) on light nuclei (…^{12}C, ^{14}N, ^{16}O, …)
  - *(p,γ) cross sections are measurable at energy as low as 100 keV and model extrapolation down to about 10 keV allows to investigate stellar hydrogen burning in massive stars, initiating the CNO cycle.*

- The elastic (p,p) cross section responds to the complex quantum nature of the nuclear interaction.
  - *In the example on the right the measured deviation from the Rutherford value of the elastic $^{12}C(p,p)^{12}C$ (170°) are clearly seen. The first resonance at about 460 keV corresponds to the S-factor resonance of the (p,γ) reaction.*

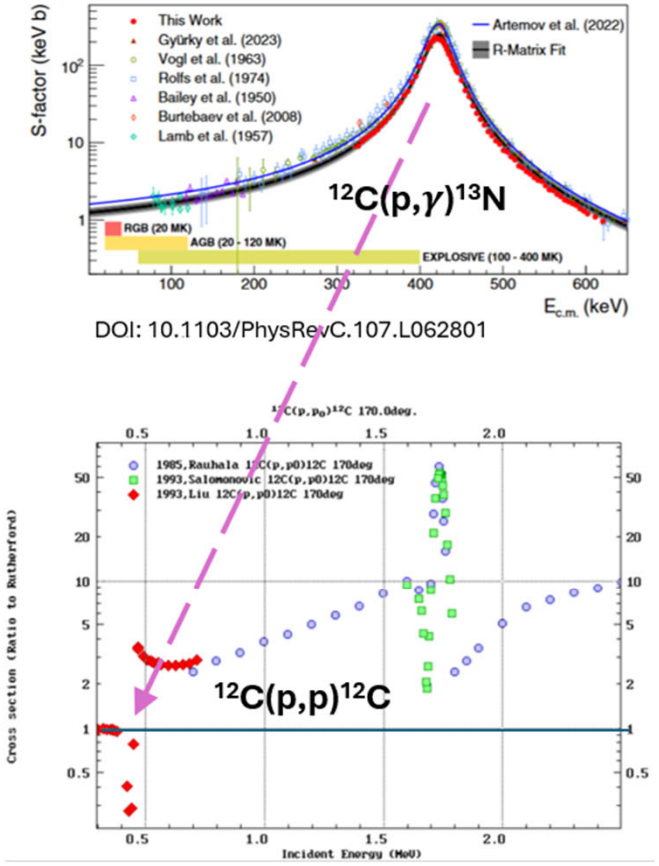

Elastic (non-Rutherford) backscattering cross section (II)

The complex elastic scattering cross section functions can be calculated from nuclear models using all available nuclear data.

The IBA and Materials Research communities, under the auspices of IAEA created the IBANDL website (https://www-nds.iaea.org/exfor/ibandl.htm), where most of existing experimental cross sections are collected.

As an example, on the right, the elastic back-scattering cross sections for p+^{16}O and α+^{16}O at 170° are shown.

- Large deviations from Rutherford are observed

In practice, the increase of cross section can be used for enhancing the sensitivity of Backscattering Yield analyses.

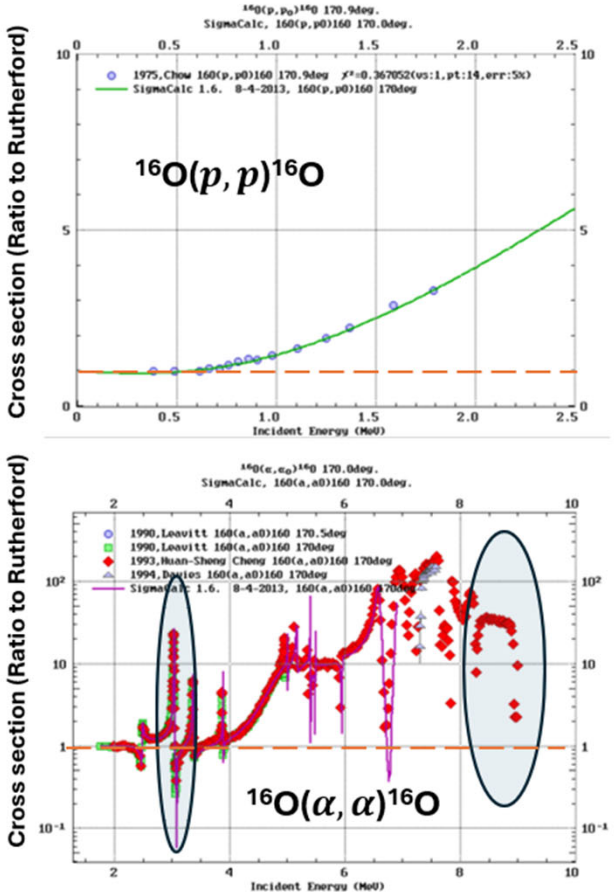

Elastic (non-Rutherford) backscattering spectra

- Example of (p,p) elastic scattering on Silicon

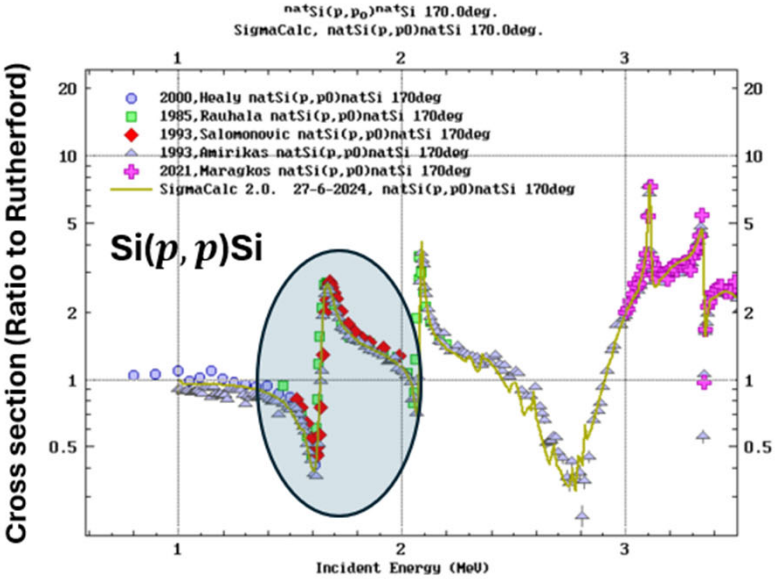

Deviates at energy higher than 1.2 MeV @170°

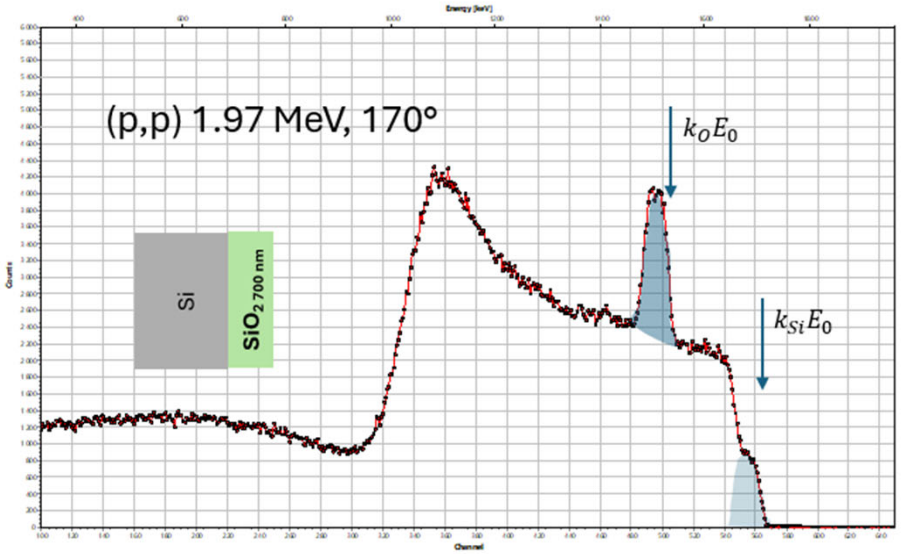

Experimental spectrum of a SiO_2 layer (700 nm) deposited onto a Silicon wafer. The profile of the non Rutherford cross section of the Silicon backing is easily recognizable.

The $^{27}Al(p,p)^{27}Al$ case

The most detailed, high resolution measurements of Al(p,p)Al are reported by Nelson et al. (Phys. Rev. C29 (1984) 1656 – see left). Differential cross sections in the energy range from 0.92 to 3.05 MeV with an overall resolution of 350 to 400 eV for several scattering angles have been measured. Gurbich et.al (NIM B190 (2002) 237) have shown that complicated resonant structure spectra (such as Al(p,p)Al) can be "*adequately*" simulated in backscattering analyses only if the excitation function is known in every detail.

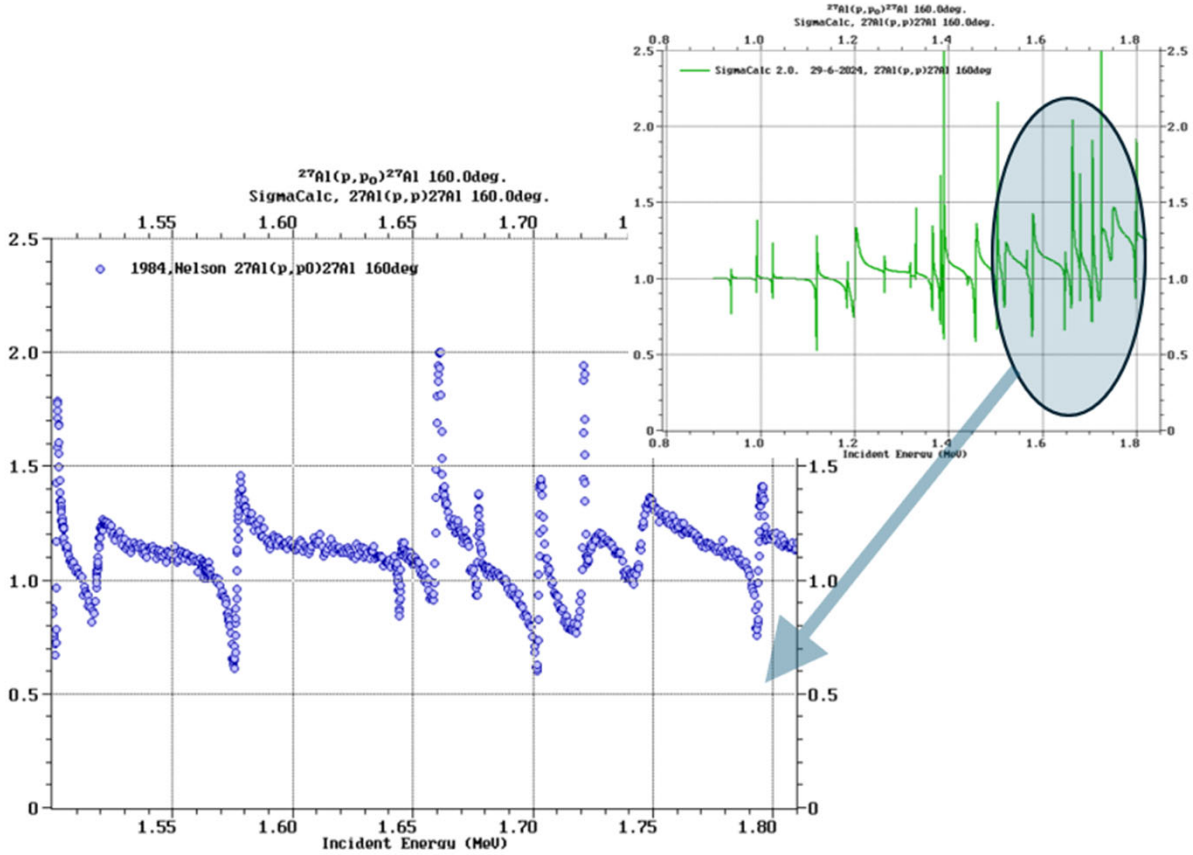

The $^{27}Al(p,p)^{27}Al$ cross section (ratio to Rutherford) in the energy range 0.8-1.8 MeV (160°) . The cross section approaches the Rutherford value at about 0.9 MeV.
R.O. Nelson et al. Physical Review, C, 29, 1656 (1984)

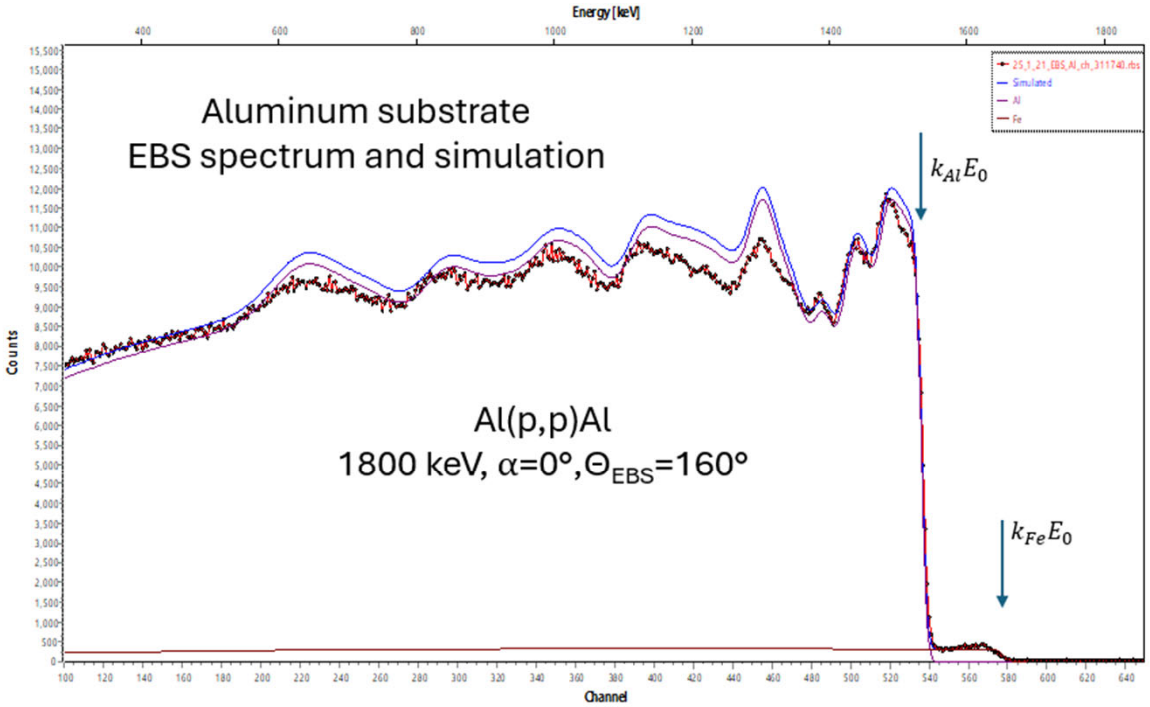

PIXE Analysis for impurity determination (proton beam 3.6 MeV)

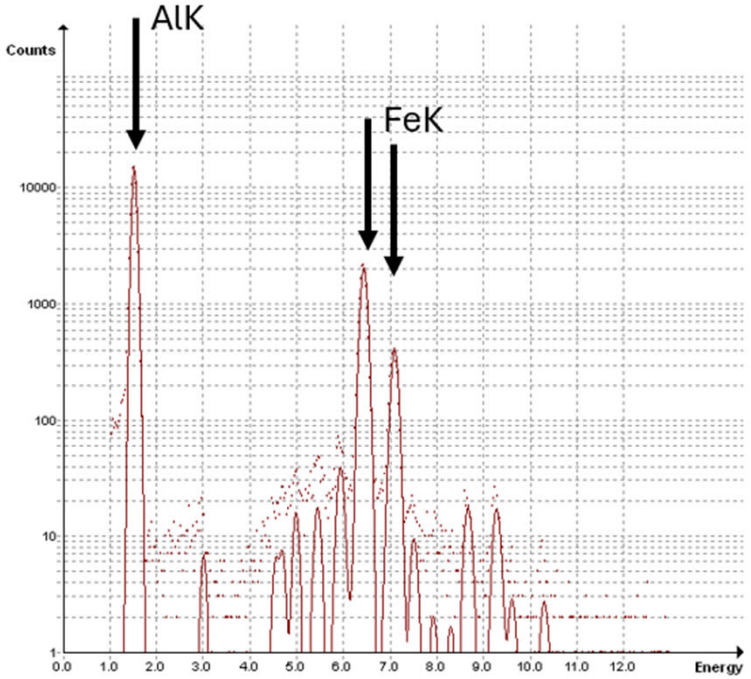

Main contaminant: Fe, about 0.1 %
other trace ppm elements: Cr, Mn, Zn, Ga

p-EBS Analysis of $^{48}TiO_x$/Al samples with roughness (AN2000, E_{nom}=1800 keV, Θ_{in}=0°, Θ_{EBS}=160°)

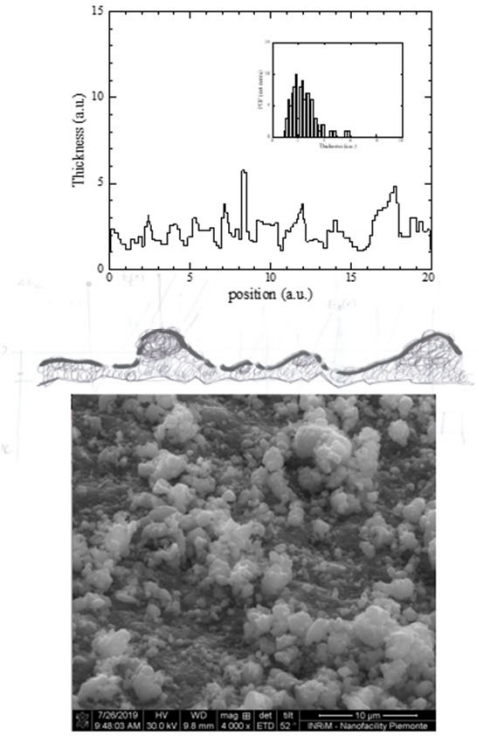

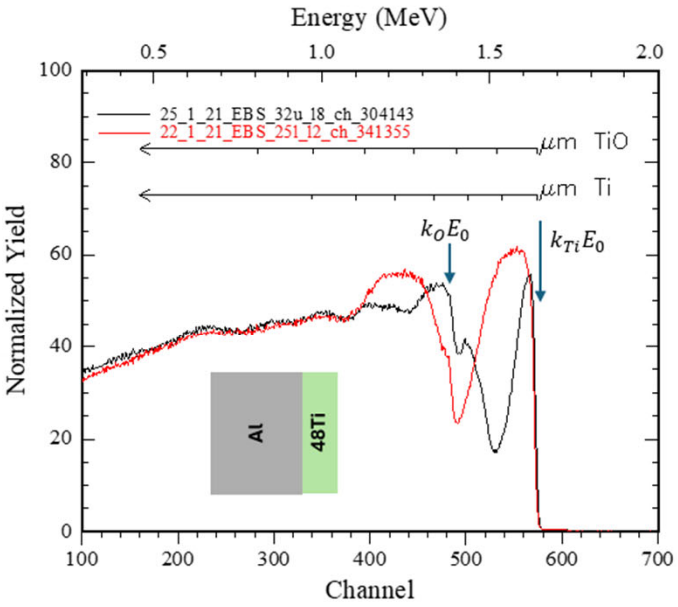

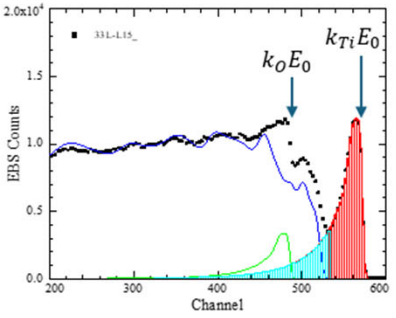

Ti, O, Al contributions are deconvoluted through an EBS simulation including roughness and non Rutherford / Rutherford cross sections

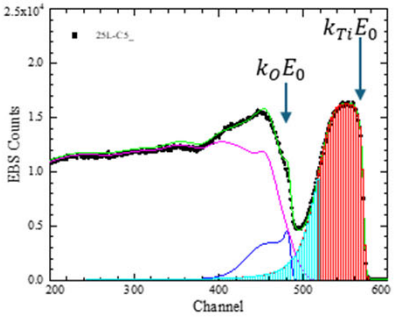

O(α,α) elastic scattering at 8.75 MeV, 170°

The dependency of the Rutherford formula from Z_2^2 will make the detection of Oxygen (Z_2=8) over a Tantalum (Z_2=73) substrate practically impossible.

At **8.75 MeV, 170°**

- the $^{16}O(^4He,^4He)^{16}O$ cross section is ≈ 30 times the Rutherford value (slide 35).
- The $Ta(^4He,^4He)$ cross section is Rutherford

It is possible, in this experimental condition, to:

- detect oxygen over tantalum directly
- separate ^{16}O from ^{17}O
- measure precisely the thickness and stoichiometry of the Ta_2O_5 layer.

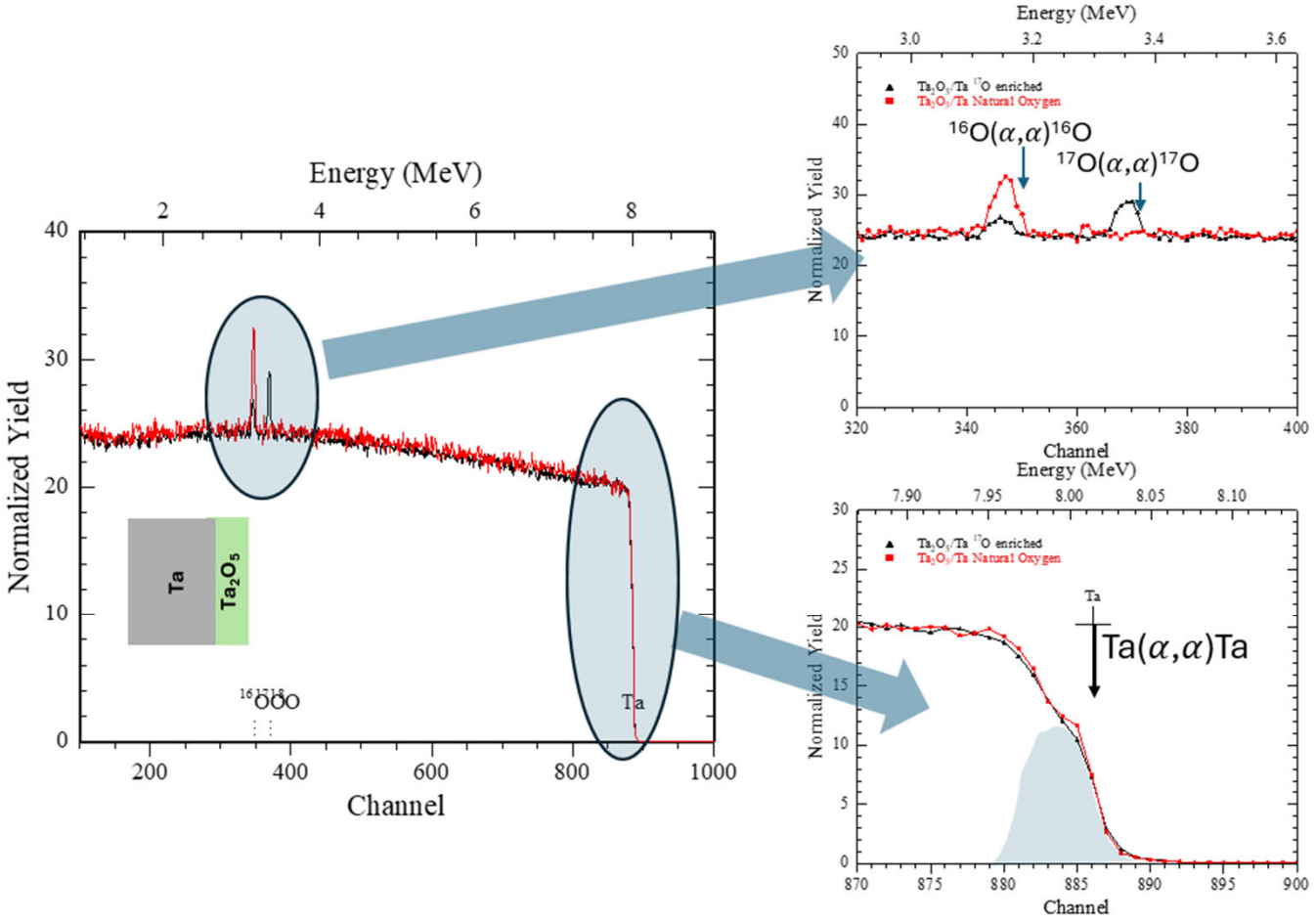

Material

- Stopping power
  - NIST: *https://www.nist.gov/pml/stopping-power-range-tables-electrons-protons-and-helium-ions*
  - SRIM2013: *http://www.srim.org/*
- Software
  - SimNRA 7: *https://mam.home.ipp.mpg.de/*
- Cross sections: *https://www-nds.iaea.org/exfor/ibandl.htm*

Other readings

- W-K Chu, J.W. Mayer, M-A Nicolet, *Backscattering Spectrometry*, Academic Press, 1978 (*Doi: https://doi.org/10.31399/asm.hb.v10.a0001775*)
- Handbook of Modern Ion Beam Materials Analysis, J.R. Tesmer, M. Nastasi ed.; MRS Pittsburgh (PA) 1995 (ISBN-10, 1605112151)

Thank for your attention!